J. Fluid Mech. (1980), *vol.* 97, *part* 3, *pp.* 531–556
Printed in Great Britain

The oblique wing as a lifting-line problem in transonic flow

By H. K. CHENG AND S. Y. MENG

Department of Aerospace Engineering,
University of Southern California, Los Angeles, California 90007

(Received 14 June 1979)

A transonic-flow theory of thin, oblique wing of high aspect ratio is presented, which permits a delineation of the influence of wing sweep, the centre-line curvature, and other three-dimensional (3D) effects on the nonlinear mixed flow in the framework of small-disturbance theory. In the (parameter) domain of interest, the flow field far from the wing section pertains to a high subsonic, or linear sonic, outer flow, representable by a Prandtl–Glauert solution involving a swept, as well as curved, lifting line in the leading approximation.

Among the 3D effects is one arising from the compressibility correction to the velocity divergence, absent in classical works; this effect also leads to a correction in the outer flow in the form of an oblique line source. More important is the upwash corrections which includes the influence of both the near and far wakes, as well as the local curvature of the centre-line. For straight oblique wings, local similarities exist in the 3D flow structure, permitting the reduced equations to be solved *once* for *all* span stations. An analogy also exists between the oblique-wing problem and that of a 2D transonic flow which is weakly time-dependent; this provides an alternative method of solving numerically the inner airfoil problem.

Solutions to the reduced problem are demonstrated and compared with full-potential solutions for elliptic oblique wings involving high subcritical as well as slightly supercritical component flows.

1. Introduction

Use of wing sweep to control the compressibility effect has long been a practice in aircraft design (Busemann 1935; Jones 1946; Jones & Cohen 1957; Küchemann 1969). Consider a high-aspect-ratio wing with a given airfoil section; there is generally a range of sweep angle (at each span station), in which the velocity component perpendicular to the (local) span is sufficiently low to permit a shock-free or nearly shock-free component flow, yet is close enough to the sonic speed for the maintenance of a high lift coefficient. In this sweep range lies the possibility for applying the two-dimensional (2D) supercritical airfoil data to aircraft design (Bauer *et al.* 1974; Nieuwland 1967; Boerstoel 1974; Kacprzynski *et al.* 1971; Whitcomb 1974). The flow field in this case is necessarily nonlinear and admits features characterizing the mixed (elliptic–hyperbolic) flow. In the present work, we study the three-dimensional (3D) structure of this nonlinear mixed flow by solving a perturbation problem and determining its solution through matching with a lifting-line solution to an outer problem.

The approach taken is that of an asymptotic theory for high-aspect-ratio planar wings and, therefore, shares a common base with the classical lifting-line theory

0022-1120/80/4418-8690 $02.00

(Prandtl 1918; Van Dyke 1964; Ashley & Landahl 1965). Apart from the nonlinear mixed flow and other compressibility effects, the following development takes into account the influence of the wing sweep, as well as the curvature of the planform's centre-line, absent in the classical work. The analysis was motivated in part by Jones' (1971, 1977) works on the straight oblique wing which offers an ideal opportunity for extending the lifting-line concept, and naturally becomes the focus of the present investigation.

Similar extensions have been made earlier by the first author in the context of unsteady incompressible flow for a curved centre-line (Cheng 1976) and of steady incompressible flow for an oblique wing (Cheng 1978*a*, *b*). The present study is carried out in a framework equivalent to the transonic small-disturbance approximation in a potential flow, with an aim of bringing about a greater simplicity in the problem analysis, which should greatly reduce computation work and shed light on the 3D structure of the transonic mixed flow. For straight oblique wings, this theory yields an analogy with an unsteady 2D flow of a thin airfoil in the nonlinear transonic regime; the formulation also admits a local similarity in the 3D structure, providing a reduction of the computation work for a rather useful class of oblique-wing geometries.

An outline of the analysis concerning the similarity solutions of the oblique wings has been sketched in a greatly condensed note (Cheng & Meng 1979*a*). This paper presents the theory in a fuller context; apart from the crucial details in the theoretical development, the work discusses comparisons of the analysis with computer solutions based on full-potential equations for oblique wings with high subcritical and slightly supercritical component flows. The theory given is valid also for a curved centre-line (see requirements below) and is expected to hold also in the more conventional case of a symmetric swept wing (cf. figure 1*c*), although without further treatment the solution is not applicable to the vicinity of the wing apex. The work is based mainly on material presented in an unpublished report under the same title (Cheng & Meng 1979*b*), where much of the analytical detail, together with numerical data, can be found.

For a straight unswept wing the 3D effect would appear mainly as a local upwash correction; Cook & Cole (1978) have given a rather complete elucidation of this problem; Cook (1978) has also studied the uniqueness of the solution to the reduced problem. With the wing sweep, two important features emerge. One is a significant upwash induced by the near-wake vorticities, which is responsible for the pronounced rolling moment characteristic of an untwisted oblique wing (see Jones 1977; see also Cheng 1978*a*); the other is an additional compressibility correction to the velocity divergence arising from the spanwise density variation (§ 2.1). On account of the latter feature, the flow field next to each wing section can no longer be treated as being planar. In formulating the inner problem, one would also have to consider the effect of the spanwise component of the near-wake vorticity. This feature does not appear, however, in the present analysis owing to the relatively small sweep angle required by the nonlinear domain (lest the inner problem becomes linear).

An interesting development in the present asymptotic theory is the uncovering of an oblique line source in the third-order lifting-line theory, unsuspected in previous works. The effect in question arises from the spanwise compressibility correction mentioned and depends on the sectional lift (nonlinearly), as well as the spanwise and chordwise distributions of the wing thickness. In passing, we observe that similar

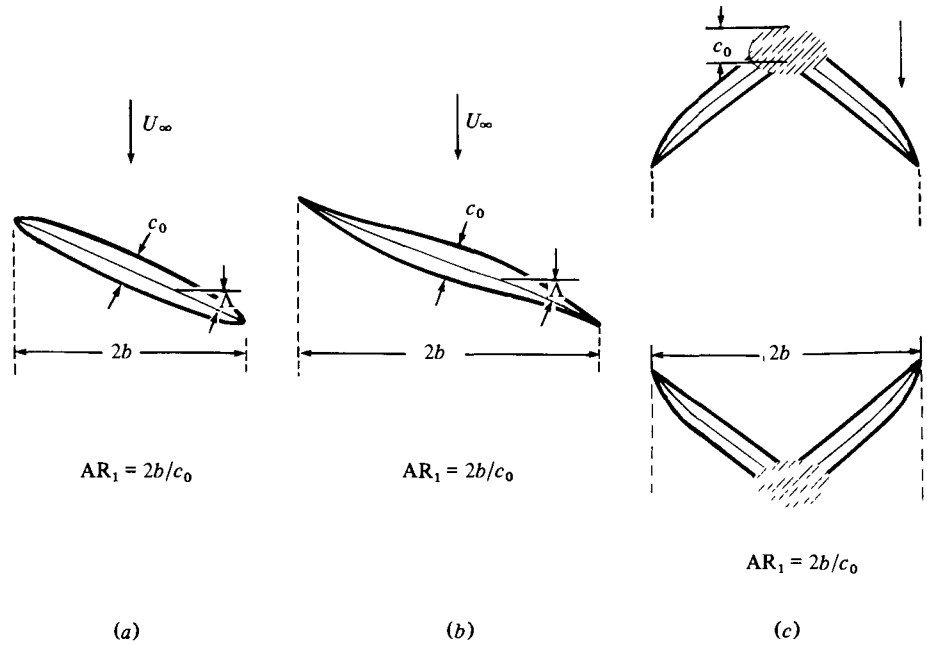

FIGURE 1. Illustration of the reference chord, the span and the aspect ratio used for a straight oblique wing (*a*), a more general curved oblique wing (*b*), and symmetric swept wings (*c*); the shaded areas in (*c*) indicates regions of breakdown. Breakdown (non-uniformity) of the theory may also occur in the tip region (cf. text).

source effects should arise in a linear problem, although the lift distributions of interest will not be affected (to the order of AR_1^{-1}) in such a case.

As is well known from Oswatitsch & Zierep's (1960) work, there is a weak singularity at the juncture of the shock and the curved portion of an impermeable surface, where the flow will undergo a re-expansion. In the perturbation part of the solution, this singularity manifests as a logarithmic singularity in the pressure distribution behind the shock root. A similar problem (of non-uniformity) occurs in the shock analysis in the context of an unsteady transonic plane flow (§ 4.1), where the difficulty is compounded by other complexities in computations and has not been fully recognized.† This problem with the re-expansion singularity is treated in § 2.4.

In the following, $2b$ denotes the wing span (measured perpendicularly to the main flow direction) and c_0 the root chord (measured perpendicularly to the centre-line); refer to figure 1. The aspect ratio is defined as $\mathrm{AR}_1 \equiv 2b/c_0$. We use α to characterize the wing camber and the angle of attack (measured from the zero-lift angle), and will assume that the wing-thickness ratio is also comparable to α. The local swept angle is Λ; the free-stream Mach number is M_∞, and the Mach number of the free-stream component flow is $M_n = M_\infty \cos\Lambda$. Three parameters will control the reduced (local) problem

$$K_n \equiv (1-M_n^2)/\alpha^{\frac{2}{3}}M_n, \quad \Theta \equiv \Lambda/\alpha^{\frac{1}{3}}, \quad \epsilon \equiv 1/\alpha^{\frac{1}{3}}\mathrm{AR}, \tag{1}$$

† The logarithmic singularity in the unsteady problem has been noted in a very recent work by Williams (1979), in which the non-uniformity has not been treated.

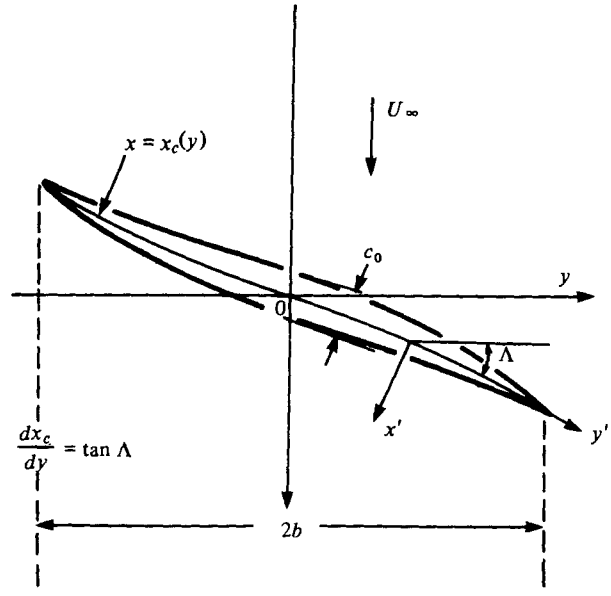

FIGURE 2. Illustration of the Cartesian and the orthogonal curvilinear co-ordinate systems in the wing plane ($x = z' = 0$).

where ϵ may be regarded as the reciprocal of a reduced aspect ratio, and Θ is a re-scaled (typical) sweep angle. The parameter K_n is essentially the transonic similarity parameter written for the component flow, with the factor in the denominator taken as the *first* power of M_n, as in Murman & Krupp (1971); this choice allows a better approximation of the critical speed (cf. § 2). The flow field next to the wing section and that removed from it are analysed as two asymptotically distinct (inner and outer) regions for $\epsilon \to 0$ with fixed K_n, Θ, and $\alpha^{\frac{1}{3}}/\epsilon$. The last quotient is fixed in order to simplify the remainder estimate. As it will become apparent later in § 3, the relative magnitude of Θ^2 and K_n will also determine whether the outer flow is (high) subsonic, (near) sonic, or (low) supersonic. Only the domain in which $\Theta^2 < K_n = O(1)$, corresponding to a high subsonic, or a linear sonic, outer flow is considered.†

2. The inner airfoil problem

2.1. *Governing equations*

We consider a steady irrotational flow of a calorically perfect gas with a uniform free stream. The partial differential equation (p.d.e.) for the perturbation velocity potential ϕ can be written in Cartesian co-ordinates (x, y, z) as

$$(1-M_\infty^2)\phi_{xx}+\phi_{yy}+\phi_{zz} = M_\infty^2 U_\infty^{-1}\frac{\partial}{\partial x}\left[\left(1+\frac{\gamma-1}{2}M_\infty^2\right)\phi_x^2+\phi_y^2+\phi_z^2\right]+\ldots, \quad (2.1)$$

† The special problem of a straight oblique wing has also been studied by Cook (1979), using oblique co-ordinates. The similitude in the 3D structure was not brought out, however. The far-field analysis therein also omits a line-source and other logarithmic terms.

where the remainder (...) consists of triple and quadruple products of ϕ, e.g. $U_\infty^2 \phi_x^2 \phi_{xx}$, etc., γ is the specific heat ratio and subscripts x, y and z signify partial derivatives.

For the analysis of the flow field in the neighbourhood of the wing section, referred to as the inner region hereafter, a right-handed curvilinear orthogonal co-ordinate system (x', y', z') will be used (refer to figure 2), in which x' and z' are distances from the centre-line (a reference curve) of the wing planform, with z' measured along a normal from the wing plane. The y' co-ordinate is then a distance measured along the (curved) centre-line. Writing Λ as the local sweep angle of the centre-line, one observes the following identities

$$dx^2+dy^2+dz^2 = dx'^2+h_2^2 dy'^2+dz'^2, \quad h_2 = 1-x'\,d\Lambda/dy', \tag{2.2}$$

$$\frac{\partial}{\partial x} = \cos\Lambda \frac{\partial}{\partial x'} + \frac{\sin\Lambda}{h_2}\frac{\partial}{\partial y'}, \quad \frac{\partial}{\partial y} = -\sin\Lambda \frac{\partial}{\partial x'} + \frac{\cos\Lambda}{h_2}\frac{\partial}{\partial y'}. \tag{2.3}$$

The p.d.e. (2.1) may then be expressed in the curvilinear co-ordinates with $U_n = U_\infty \cos\Lambda$ and $M_n = M_\infty \cos\Lambda$. In anticipation of a transonic component flow, we normalize x', z', y' and ϕ as follows

$$\hat{x} = \frac{2x'}{c_0}, \quad \hat{z} = 2M_n\left(\frac{\alpha}{M_n}\right)^{\frac{1}{3}}\frac{z'}{c_0}, \quad \hat{y} = \frac{y'}{b}, \quad \hat{\phi} = \frac{2\phi}{(\alpha/M_n)^{\frac{1}{3}} U_n c_0}. \tag{2.4}$$

Except for the trivial differences of using a half chord $\frac{1}{2}c_0$ instead of c_0 and omitting factors with $(\gamma+1)$, the resulting variables can be identified with those in the earlier works on the small-disturbance theory of plane transonic flow (Sprieter 1953; also see Ashley & Landahl 1965).

Using these variables, and eliminating $(1-M_n^2)$, $\tan\Lambda$, and c_0/b through K_n, $\alpha^{\frac{1}{3}}/\epsilon$ and Θ, (2.1) can be reduced to

$$\frac{\partial}{\partial\hat{x}}\left[K_n\hat{\phi}_{\hat{x}} - \frac{\gamma+1}{2}\hat{\phi}_{\hat{x}}^2\right] + \hat{\phi}_{\hat{z}\hat{z}} = \epsilon\left[2\Theta\frac{\partial}{\partial\hat{y}} + \Theta'\right]\hat{\phi}_{\hat{x}} + \ldots, \tag{2.5}$$

where Θ' is $d\Theta/d\hat{y}$, the terms omitted (...) belong to orders ϵ^2 and $\alpha^{\frac{2}{3}}$ under the stipulation of a finite K_n and Θ, or simply order ϵ^2 for finite K_n, Θ and $\alpha^{\frac{1}{3}}/\epsilon$. The pressure perturbation can be computed from $\hat{\phi}_{\hat{x}}$ as

$$c_p' \equiv (p-p_\infty)/\tfrac{1}{2}\rho_\infty U_n^2 = -2\left(\frac{\alpha}{M_n}\right)^{\frac{2}{3}}\hat{\phi}_{\hat{x}} + \ldots \tag{2.6}$$

subject to an error comparable to ϵ^4. The retention of the factor M_n in the definition of K_n and scaling factors for $\hat{\phi}$ and $\hat{z}$, as well as the factor $\cos\Lambda$ in $U_n = U_\infty\cos\Lambda$ of (2.4) and (2.6), are not fundamental from the viewpoint of an asymptotic theory. Our preference for these choices will be explained later.†

For the present study, we consider impermeable wing surfaces prescribed over the planform $\hat{a}(y) < \hat{x} < \hat{b}(y)$ as

$$z' = \frac{c_0}{2}[\alpha\hat{Z}^{\pm}(\hat{x},\hat{y}) + \alpha^{\frac{1}{3}}\hat{Z}_B(\hat{y}) + \alpha\epsilon(\hat{x}-\hat{x}_0)\hat{I}(\hat{y})], \tag{2.7}$$

where $\hat{a}$ and $\hat{b}$ locate the leading and trailing edge, respectively, the superscripts '+' and '−' refer to the upper and lower surfaces, respectively, and $\hat{Z}$, $\hat{Z}_B$ and $\hat{I}$ are all of unit order. The function $\hat{I}(\hat{y})$ and $\hat{Z}_B(\hat{y})$ signify, respectively, a wing twist and an

† These factors M_n and $\cos\Lambda$ were not used in the definitions of K_n, and $\hat{z}$ in our earlier note (Cheng & Meng 1979*a*).

upward wing bending; both $\hat{Z}_B$ and $\hat{l}$ have been scaled in a way to allow the control of the three-dimensional effects (see below). The boundary condition on the wing can be transferred to the wing plane ($\hat{z} = 0$) as

$$(\partial\hat{\phi}/\partial\hat{z})_w = \frac{\partial}{\partial\hat{x}}\hat{Z}^{\pm} + \epsilon\Theta\hat{Z}'_B + \epsilon\hat{l} + \ldots \tag{2.8}$$

where $\hat{Z}'_B$ is $d\hat{Z}_B/d\hat{y}$ and the subscript 'w' refers to points on the wing plane bounded by $\hat{a} < \hat{x} < \hat{b}$. We assume that in approaching the leading edge, $Z^{\pm} \sim \pm$ const. $(\hat{x}-\hat{a})^{\frac{1}{2}}$. Except at the leading and trailing edges, the remainder (...), including errors from the boundary-condition transfer, belong to orders $\alpha^{\frac{3}{2}}$ or ϵ^2, same as in (2.5). The pressure and the velocity component normal to the trailing-vortex sheet is required to be continuous across the sheet. These conditions are again transferred to $\hat{z} = 0$ to read, subject to error comparable to ϵ^2,

$$[\![\hat{\phi}_{\hat{x}}]\!]_{\mathrm{TV}} = [\![\hat{\phi}_{\hat{z}}]\!]_{\mathrm{TV}} = 0, \tag{2.9}$$

where $[\![\ ]\!]_{\mathrm{TV}}$ signifies the difference across the trailing vortex (TV) sheet behind the wing. The first of (2.9) indicates that the cross-stream vorticity of the near wake is unimportant. The streamwise vorticity component of the near wake will, nevertheless, be shown in § 3 to be very significant.

The reduced p.d.e. comprised of all terms shown in (2.5) has the characteristics $\hat{x} = \hat{x}^C(\hat{y},\hat{z})$ satisfying (Courant & Hilbert 1965)

$$K_n - (\gamma+1)\hat{\phi}_{\hat{x}} + 2\epsilon\Theta\frac{\partial\hat{x}^C}{\partial\hat{y}} = -\left(\frac{\partial\hat{x}^C}{\partial\hat{z}}\right)^2; \tag{2.10}$$

its existence as a real surface requires

$$K_n - (\gamma+1)\hat{\phi}_{\hat{x}} + 2\epsilon\Theta\frac{\partial\hat{x}^C}{\partial\hat{y}} < 0. \tag{2.11}$$

The limit $\epsilon \to 0$ (with finite Θ and K_n) determines a critical speed for the 2D component flow

$$\hat{\phi}_{\hat{x}} = K_n/(\gamma+1) \equiv \hat{u}_*. \tag{2.12}$$

This identifies the transition boundary of the hyperbolic and the elliptic regions, and is also the locus where the 2D *component velocity* reaches the sonic speed – a fact familiar from the transonic small-disturbance theory for the *plane* flow.

Partial differential equation (2.5) and the equations expressing irrotationality admit weak solutions with a surface of discontinuity in $\nabla\phi$, say $\hat{x} = \hat{x}^D(\hat{y},\hat{z})$, identifiable with gasdynamic shock waves. The shock conditions admissible to the weak solution and consistent with Rankine–Hugonoit relations, can be written as, at $\hat{x} = \hat{x}^D(\hat{y},\hat{z})$,

$$K_n - (\gamma+1)\langle\hat{\phi}_{\hat{x}}\rangle + 2\epsilon\Theta\frac{\partial\hat{x}^D}{\partial\hat{y}} = -\left(\frac{\partial\hat{x}^D}{\partial\hat{y}}\right)^2, \tag{2.13a}$$

$$[\![\hat{\phi}]\!] = 0 \tag{2.13b}$$

where, $\langle\ \rangle$ and $[\![\ ]\!]$ stand for the arithmetical mean and the jump of the quantity across the surface in question, respectively. The continuity of $\hat{\phi}$ (2.13b), implies the continuity of the tangential velocities,

$$[\![\hat{\phi}_{\hat{x}}]\!] : [\![\hat{\phi}_{\hat{z}}]\!] : [\![\hat{\phi}_{\hat{y}}]\!] = -1 : \frac{\partial\hat{x}^D}{\partial\hat{z}} : \frac{\partial\hat{x}^D}{\partial\hat{y}}.$$

We observe that higher-order terms delected from the coefficient of $\hat{\phi}_{\hat{x}\hat{x}}$ in (2.5) cause incorrect description of the characteristic slopes near the transition boundary and are expected to lead to a non-uniformity at some stage of the high-order expansion of the inner solution. This deficiency can be removed through a correction to the critical speed $\hat{u}_*$, hence K_n, to the basic *component* flow. The result can be cast in a form of a slightly modified definition for the similarity parameter, subject to error of the order $(1-M_n)^2$ or $O(\epsilon^4)$ (Cheng & Meng 1979*b*, appendix I). Namely, writing K_n in (2.5) as

$$K_n' \equiv (1-M_n^2)/\alpha^{\frac{2}{3}} M_n^{\omega}, \tag{2.14a}$$

with

$$\omega = (4\gamma+1)/3(\gamma+1). \tag{2.14b}$$

Since ω is reasonably close to one, ranging from $\frac{5}{6}$ for $\gamma = 1$ to $\frac{23}{24}$ for $\gamma = \frac{5}{3}$, we therefore take ω to be *unity* in our definition for K_n. We also point out that $U_n = U_\infty \cos\Lambda$ used in the definition of $\hat{\phi}$ and c_p' could be replaced by U_∞, incurring errors no larger than $O(\epsilon^2)$ or $O(\alpha^{\frac{2}{3}})$, since $\Lambda = O(\alpha^{\frac{1}{3}})$ for $\Theta = O(1)$. However, its retention in the leading approximation of ϕ and in c_p' has an advantage for enlarging slightly the range of the applicability for the sweep angle. It is shown (Cheng & Meng 1979*b*) that, with the retention of $\cos\Lambda$, Θ can be extended to $\Theta = O(\epsilon^{-\frac{1}{2}})$ without incurring larger errors.

2.2. *Perturbation of the component flow*

Equations (2.5), (2.8) and (2.9) permit an expansion of $\hat{\phi}$ in ϵ

$$\hat{\phi} = \hat{\phi}_0 + \epsilon\hat{\phi}_1 + \ldots, \tag{2.15}$$

where a weak (logarithmic) dependence of $\hat{\phi}_1$ on ϵ is anticipated. The leading term $\hat{\phi}_0$ is a 2D solution to the component flow at the span station $\hat{y}$ satisfying the p.d.e. and the conditions on the x axis:

$$\left[K_n - (\gamma+1)\frac{\partial}{\partial\hat{x}}\hat{\phi}_0\right]\frac{\partial^2}{\partial\hat{x}^2}\hat{\phi}_0 + \frac{\partial^2}{\partial\hat{z}^2}\hat{\phi}_0 = 0, \tag{2.16}$$

$$\left(\frac{\partial}{\partial\hat{z}}\hat{\phi}_0\right)_w = \frac{d}{d\hat{y}}\hat{Z}^{\pm}; \quad \left[\!\left[\frac{\partial}{\partial\hat{x}}\hat{\phi}_0\right]\!\right]_{\mathrm{TV}} = \left[\!\left[\frac{\partial}{\partial\hat{z}}\hat{\phi}_0\right]\!\right]_{\mathrm{TV}} = 0, \tag{2.17}$$

where the subscripts 'w' and 'TV' have the same meaning as before. The coefficient $\hat{\phi}_1$ is governed by the linear non-homogeneous p.d.e. and boundary conditions in variables $\hat{x}$ and $\hat{z}$, obtained after equating terms proportional to the first power ϵ:

$$\left[K_n - (\gamma+1)\frac{\partial}{\partial\hat{x}}\hat{\phi}_0\right]\frac{\partial^2}{\partial\hat{x}^2}\hat{\phi}_1 + \frac{\partial^2}{\partial\hat{z}^2}\hat{\phi}_1 - (\gamma+1)\frac{\partial^2}{\partial\hat{x}^2}\hat{\phi}_0\frac{\partial}{\partial\hat{x}}\hat{\phi}_1 = \left[2\Theta\frac{\partial}{\partial\hat{y}} + \Theta'\right]\frac{\partial}{\partial\hat{x}}\hat{\phi}_0, \tag{2.18}$$

$$\left(\frac{\partial}{\partial\hat{z}}\hat{\phi}_1\right)_w = \Theta\frac{d}{d\hat{y}}\hat{Z}_B, \quad \left[\!\left[\frac{\partial}{\partial\hat{x}}\hat{\phi}_1\right]\!\right]_{\mathrm{TV}} = \left[\!\left[\frac{\partial}{\partial\hat{z}}\hat{\phi}_1\right]\!\right]_{\mathrm{TV}} = 0, \tag{2.19}$$

where $\hat{y}$ appears essentially as a parameter. The solutions $\hat{\phi}_1$ and $\hat{\phi}_0$ share the same characteristics system $\hat{x} = \hat{x}_0^C(\hat{y},\hat{z})$ described by

$$K_n - (\gamma+1)\frac{\partial}{\partial\hat{x}}\hat{\phi}_0 = -\left(\frac{\partial\hat{x}_0^C}{\partial\hat{z}}\right)^2, \tag{2.20}$$

with the transition boundary separating the elliptic and hyperbolic being

$$K_n-(\gamma+1)\frac{\partial}{\partial\hat{x}}\hat{\phi}_0=0$$

for both.

The equation describing the shock is expanded as

$$\hat{x}=\hat{x}^D(\hat{y},\hat{z})=\hat{x}_0^D(\hat{y},\hat{z})+\epsilon\hat{x}_1^D(\hat{y},\hat{z})+\ldots, \tag{2.21}$$

allowing again a weak (logarithmic) dependence of $\hat{x}_1^D$ on ϵ. The jump relations (2.13) can be transferred from $\hat{x}=\hat{x}^D$ to $\hat{x}=\hat{x}_0^D$, yielding, after equating terms of equal algebraic powers of ϵ,

$$K_n-(\gamma+1)\left\langle\frac{\partial}{\partial\hat{x}}\hat{\phi}_0\right\rangle=-\left(\frac{\partial\hat{x}_0^D}{\partial\hat{z}}\right)^2,\quad [\![\hat{\phi}_0]\!]=0; \tag{2.22}$$

$$\left.\begin{aligned}2\Theta\frac{\partial\hat{x}_0^D}{\partial\hat{y}}-(\gamma+1)\left\langle\frac{\partial}{\partial\hat{x}}\hat{\phi}_1+\hat{x}_1\frac{\partial^2}{\partial\hat{x}^2}\hat{\phi}_0\right\rangle&=-2\frac{\partial\hat{x}_0^D}{\partial\hat{z}}\frac{\partial\hat{x}_1^D}{\partial\hat{z}},\\ \left[\!\!\left[\hat{\phi}_1+\hat{x}_1\frac{\partial}{\partial\hat{x}}\hat{\phi}_0\right]\!\!\right]&=0.\end{aligned}\right\} \tag{2.23}$$

As noted earlier, the subcritical flow right behind the shock root over a curved (wing) surface has a weak singularity in the surface value of $(\hat{\phi}_0)_{\hat{x}}$ like

$$(\hat{x}-\hat{x}_0^D)\ln|\hat{x}-\hat{x}_0^D|,$$

this will then give a logarithmic singularity in $\hat{\phi}_{1\hat{x}}$, in view of the jump condition (2.23). This non-uniformity is discussed in § 2.4.

2.3. *Behaviour at large distance*

Since $\partial\hat{\phi}_0/\partial\hat{x}$ vanishes as $|\hat{\zeta}|\equiv(\hat{x}^2+K_n\hat{z}^2)^{\frac{1}{2}}\to\infty$, p.d.e. (2.16) under $K_n>0$ approaches a Laplace equation in $\hat{x}$ and $\hat{\eta}\equiv K_n^{\frac{1}{2}}\hat{z}$; the leading term in an asymptotic expansion for $\hat{\phi}_0$ at large $|\hat{\zeta}|$ may therefore be represented by a vortex potential in the variable $\hat{\zeta}\equiv\hat{x}+i\hat{\eta}$. This and the successive terms in the development of $\hat{\phi}_0$ for $|\hat{\zeta}|\gg1$ can be inferred from p.d.e. (2.16) under the requirement that $(\hat{\phi}_0)_{\hat{x}}$ and $(\hat{\phi}_0)_\eta$ are continuous everywhere including the $\hat{x}$ axis (removed from the wing section)

$$\begin{aligned}\hat{\phi}_0\sim\frac{\hat{\Gamma}_0}{2\pi}\left[\tan^{-1}\left(\frac{\hat{x}}{K_n^{\frac{1}{2}}\hat{z}}\right)+\frac{\pi}{2}\operatorname{sgn}(\hat{z})\right]+\frac{\gamma+1}{4K_n}\left(\frac{\hat{\Gamma}_0}{2\pi}\right)^2\left[\ln|\hat{\zeta}|+K_n\frac{\hat{z}^2}{|\hat{\zeta}|^2}\right]\frac{\hat{x}}{|\hat{\zeta}|^2}\\ +[\hat{D}_0^r\hat{x}+\hat{D}_0^iK_n^{\frac{1}{2}}\hat{z}]\frac{1}{|\hat{\zeta}|^2}+\ldots,\end{aligned} \tag{2.24}$$

where $\hat{\Gamma}_0\equiv[\![\hat{\phi}_0]\!]$ is the circulation determined by the potential jump at the trailing edge (TE), and the remainder $(\ldots)$ is at most of the order $(\ln|\hat{\zeta}|)^2|\hat{\zeta}|^{-2}$. The coefficients $\hat{D}_0^r$ and $\hat{D}_0^i$ may be taken as the real and imaginary parts of a complex doublet strength $\hat{D}_0=\hat{D}_0^r+i\hat{D}_0^i$; they are functionals of $[\![(\hat{\phi}_0)_x]\!]_w$, $[\![\hat{Z}]\!]_w$ and $(\hat{\phi}_x)^2$, unaffected by the presence of an imbedded shock. A form comparable to (2.24) has been given earlier by Cole (1975). For numerical analysis, the explicit forms for the doublet strengths are unnecessary, since they can be determined along with solutions at and near the far boundary, with the help of a least-square method (§ 5), as has been done in Hafez & Cheng (1977*a*, *b*).

The p.d.e. (2.18) governing $\hat{\phi}_1$ approaches a Poisson equation at large $|\xi|$, providing the two leading terms in the expansion of $\hat{\phi}_1$. These and the successive terms fulfilling the continuity requirements on $\hat{\phi}_{\hat{x}}$ and $\hat{\phi}_{\hat{z}}$ can be determined, for $|\xi| \gg 1$, as

$$\begin{aligned}\hat{\phi}_1 \sim{}& \frac{\Theta\hat{z}}{K_n^{\frac{1}{2}}}\left[\left(\frac{d}{d\hat{y}}+\frac{1}{2}\frac{K_0}{K_n}\frac{\Theta'}{\Theta}\right)\frac{\hat{\Gamma}_0}{2\pi}\ln|\xi|+\frac{\Theta\Theta'}{2}\frac{\hat{\Gamma}_0}{2\pi}\frac{\hat{z}^2}{|\xi|^2}\right]-\hat{\mathbb{C}}_1^i K_n^{\frac{1}{2}}\hat{z}+\hat{\mathbb{C}}_1^r\hat{x}\\ &+\hat{N}_1+\frac{Q_1}{2\pi}\ln|\xi|+\frac{\Theta\Theta'}{2K_n}\frac{\hat{z}^2}{|\xi|^4}[\hat{D}_0^r(\hat{x}^2-K_n\hat{z}^2)+2K_n^{\frac{1}{2}}\hat{D}_0^i\hat{x}\hat{z}]\\ &+\frac{\Theta}{K_n^{\frac{1}{2}}}\frac{\hat{z}}{|\xi|^2}\left[\hat{x}\left(\frac{d}{d\hat{y}}+\frac{1}{2}\frac{K_0}{K_n}\frac{\Theta'}{\Theta}\right)\hat{D}_0^i-K_n^{\frac{1}{2}}\hat{z}\left(\frac{d}{d\hat{y}}+\frac{1}{2}\frac{K_0}{K_n}\frac{\Theta'}{\Theta}\right)\hat{D}_0^r\right]\\ &+\frac{\hat{\Gamma}_1}{2\pi}\left[\tan^{-1}\left(\frac{\hat{x}}{K_n^{\frac{1}{2}}\hat{z}}\right)+\frac{\pi}{2}\operatorname{sgn}\hat{z}\right]+\hat{F}(\hat{y})+\ldots,\end{aligned} \tag{2.25}$$

where $\hat{\Gamma}_1$ is $[\![\phi_1]\!]_{\mathrm{TE}}$; $\hat{\mathbb{C}}_1^i$ and $\hat{\mathbb{C}}_1^r$ correspond, respectively, to the induced upwash and a component-Mach-number correction to be determined later through matching; the parameter $K_0 \equiv K_n - \Theta^2$ can be identified as the transonic similarity parameter at zero sweep $(1-M_\infty^2)/\alpha_1^{\frac{2}{3}}M_\infty$. The remainder $(\ldots)$ vanishes as $|\xi| \to \infty$, and the symbol $\hat{N}_1$ designates terms arising from *nonlinear* corrections in the far field of order $(\ln|\xi|)^2$, $\ln|\xi|$, and unity:

$$\begin{aligned}\hat{N}_1 \sim{}& \frac{\gamma+1}{32}\frac{\Theta}{K_n^2}\frac{\hat{\Gamma}_0}{2\pi}\left(\frac{d}{d\hat{y}}+\frac{1}{2}\frac{\Theta'}{\Theta}\right)\hat{\Gamma}_0\left[2\ln(|\xi|)^2+2\left(\frac{2\hat{x}^2}{|\xi|^2}-1\right)(\ln|\xi|+\tfrac{1}{2})\right.\\ &\left.-\tfrac{1}{2}\left(1-8K_n\frac{\hat{z}^2\hat{x}^2}{|\xi|^4}\right)\right]+\frac{\gamma+1}{16}\frac{\Theta^2\Theta'}{K_n^3}\left(\frac{\hat{\Gamma}_0}{2\pi}\right)^2\left\{-20(\ln|\xi|)^2\right.\\ &+\left[\left(\frac{\xi}{\xi_*}\right)^2+\left(\frac{\xi_*}{\xi}\right)^2-12\left(\frac{\xi}{\xi_*}\right)-12\left(\frac{\xi_*}{\xi}\right)\right]\ln|\xi|\\ &\left.-\frac{1}{3}\left(\frac{\xi}{\xi_*}\right)^3-\frac{1}{3}\left(\frac{\xi_*}{\xi}\right)^3+\frac{5}{4}\left(\frac{\xi}{\xi_*}\right)^2+\frac{5}{4}\left(\frac{\xi_*}{\xi}\right)^2+\frac{\xi}{\xi_*}+\frac{\xi_*}{\xi}\right\},\end{aligned} \tag{2.26}$$

where ξ_* is the complex conjugate of ξ. The appearance of the source term in the far field with a strength $\hat{Q}_1 \neq 0$ should not be too surprising, since (2.18), cast into a Poisson equation

$$4\frac{\partial^2}{\partial\xi\,\partial\xi_*}\hat{\phi}_1=\left[2\Theta\frac{\partial}{\partial\hat{y}}+\Theta'\right]\frac{\partial}{\partial\hat{x}}\hat{\phi}_0+(\gamma+1)\frac{\partial}{\partial\hat{x}}[(\hat{\phi}_0)_{\hat{x}}(\hat{\phi}_1)_{\hat{x}}], \tag{2.27}$$

indicates clearly a source distribution which leads to a non-vanishing total *volume* flux to the *component* flow.

The influence of this term on the outer flow is quite similar to the one in the transonic equivalence rule involving lift (Cheng & Hafez, 1975) although the line-source effect has a considerably greater influence therein. The source strength $\hat{Q}_1$ is completely determined by the far-field property of $\hat{\phi}_0$, more specifically, $\hat{D}_0^r$ and $(\hat{\Gamma}_0)^2$.

In the case where $(\Gamma_0)^2$ can be neglected, the area integral of right-hand side (2.27) over $\hat{x}$ and η can be correctly equated to the total volume flux and determined as

$$\begin{aligned}\hat{Q}_1 &= \frac{2\Theta}{K_n}\int\int\left(\frac{\partial}{\partial\hat{y}}+\frac{\Theta'}{2\Theta}+\frac{\Theta\Theta'}{K_n}\hat{\eta}\frac{\partial}{\partial\hat{\eta}}\right)\frac{\partial}{\partial\hat{x}}\hat{\phi}_0\,d\hat{x}\,d\hat{\eta}\\ &= \frac{2\Theta}{K_n}\lim_{|\xi|\to\infty}\oint\left(\frac{\partial}{\partial\hat{y}}+\frac{\Theta'}{2\Theta}+\frac{\Theta\Theta'}{K_n}\hat{\eta}\frac{\partial}{\partial\hat{\eta}}\right)\hat{\phi}_0\,d\hat{\eta}\\ &= \frac{2\Theta}{K_n}\left[\frac{\partial}{\partial\hat{y}}+\frac{1}{2}\frac{K_0}{K_n}\frac{\Theta'}{\Theta}\right]\pi\hat{D}_0^r,\end{aligned} \tag{2.28}$$

confirming the existence of a $\hat{Q}_1 \neq 0$ (unless $\hat{D}_0^r$ or the wing thickness vanishes). For $\hat{\Gamma}_0 \neq 0$, (2.25) shows that $|\hat{\phi}_1| \gg \ln|\xi|$ and $\hat{Q}_1$ in this case cannot be evaluated simply from the area integral of right-hand side (2.18), which may be unbounded; the quantity of interest may nevertheless be determined by constructing first functions $\hat{\phi}_{0c}$ and $\hat{\phi}_{1c}$ which satisfy two Poisson equations and agree with $\hat{\phi}_0$ and $\hat{\phi}_1$, respectively, in the far field in accordance with (2.24) and (2.25); and applying next a result of Green's theorem to the difference of $(\hat{\phi}_0+\epsilon\hat{\phi}_1)$ and $(\hat{\phi}_{0c}+\epsilon\hat{\phi}_{1c})$. Using (2.13), the result can be shown to be unaffected by the presence of shocks. The explicit relation connecting $\hat{Q}_1$ to $\hat{D}_0^r$ and $(\Gamma_0)^2$ will be given in § 4 in the case of straight oblique wings under local similarity (its derivation is described in appendix III, Cheng & Meng 1979*b*).

The demonstration in (2.28) indicates that similar line-source effect will arise in the corresponding lifting-line theory in a linear subsonic flow, although the lifting and the thickness problems in this case can be separately analyzed on account of the linearity.

It is assumed that the solutions $\hat{\phi}_0$ and $\hat{\phi}_1$ are uniquely determined after fulfilling the Kutta condition at the trailing edge, the conditions (2.17), (2.19), (2.22), (2.23), and the far-field behaviour represented by the leading groups of terms on right-hand side (2.24) and right-hand side (2.25). The latters are

$$\left.\begin{aligned}\hat{\phi}_0 &\sim \frac{\hat{\Gamma}_0}{2\pi}\left[\tan^{-1}\left(\frac{\hat{x}}{K_n^{\frac{1}{2}}\hat{z}}\right)+\frac{\pi}{2}\operatorname{sgn}\hat{z}\right];\\ \hat{\phi}_1 &\sim \frac{\Theta\hat{z}}{K_n^{\frac{1}{2}}}\left[\left(\frac{d}{d\hat{y}}+\frac{1}{2}\frac{K_0}{K_n}\frac{\Theta'}{\Theta}\right)\frac{\hat{\Gamma}_0}{2\pi}\ln|\xi|+\frac{\Theta\Theta'}{2}\frac{\hat{\Gamma}_0}{2\pi}\frac{\hat{z}^2}{|\xi|^2}\right]-\hat{\mathbb{C}}_1^i K_n^{\frac{1}{2}}\hat{z}+\hat{\mathbb{C}}_1^r\hat{x}.\end{aligned}\right\} \tag{2.29}$$

The first of (2.29) is equivalent to the vanishing of the gradient of $\hat{\phi}_0$ and the second requires the specifications of the upwash and component Mach number corrections.

2.4. *The non-uniformity at the shock root*

Recall that the logarithmic singularity in $(\hat{\phi}_1)_{\hat{x}}$ is a result of the break down of the analytic continuation of $\langle(\hat{\phi}_0)_{\hat{x}}\rangle$ from the perturbed to the unperturbed shock boundaries, cf. (2.23). It is apparent that terms like $\frac{1}{2}(\hat{x}_1^D)^2\langle\hat{\phi}_{0\hat{x}\hat{x}\hat{x}}\rangle$ and $\hat{x}_2\langle\hat{\phi}_{1\hat{x}\hat{x}}\rangle$ will arise in the corresponding shock relations in the next order. This and similar reasons lead to the expectation that $(\hat{\phi}_2)_{\hat{x}}$ is singular like $1/\hat{x}$, $(\partial/\partial\hat{x})\,\hat{\phi}_3$ singular like $1/\hat{x}^2$, and so on. Thus a non-uniformity of the expansion (2.19) is identified at $\hat{x}-\hat{x}_0^D = O(\epsilon)$.

It is quite readily shown (§ 2.6, Cheng & Meng 1979*b*) from the composite system (2.5), (2.8), (2.9) and (2.13*a*, *b*) that the *form* of re-expansion singularity in $\hat{\phi}_{\hat{x}}$, written in co-ordinates fixed to the shock root, is unaffected by the 3D (as well as unsteady)

influence. This description can, therefore, be identified with the (inner) solution pertaining to the vicinity of the shock root. Let

$$\zeta \equiv \xi + i\eta; \quad \xi \equiv \frac{(Z''_w)_{\rm sr}(\hat{x} - \hat{x}^D_{\rm sr})}{\left(\frac{\gamma+1}{2}\right)^{\frac{1}{2}} |[\![\hat{u}]\!]_{\rm sr}|^{\frac{3}{2}}}, \quad \eta \equiv \frac{(Z''_w)_{\rm sr}\hat{z}^2}{|[\![\hat{u}]\!]_{\rm sr}|}, \tag{2.30}$$

where the subscript 'sr' refers to the shock root and (Z''_w) abbreviates for $\partial^2\hat{z}^{\pm}/\partial\hat{x}^2$. The description of $\hat{u} \equiv \hat{\phi}_{\hat{x}}$ in question is, $|\hat{\xi}| \ll 1$,

$$\frac{\hat{u} - \hat{u}^+_{\rm sr}}{[\![\hat{u}]\!]_{\rm sr}} \sim \text{R.P.}\left[\frac{4}{\pi}\zeta \ln\left(\frac{\zeta}{\kappa_1}\right) - i\zeta\right], \tag{2.31a}$$

where '+' refers to the post-shock condition. The corresponding form for the shock geometry is

$$\xi \sim \eta^2\left[\frac{2}{\pi}\ln\left(\frac{\eta}{\kappa_1}\right) + \mu\right], \tag{2.31b}$$

where κ_1 is an undetermined constant which is related to the location where the speed becomes a maximum, and μ is a constant determined by $[\![\hat{u}]\!]_{\rm sr}$, $(Z'_w)_{\rm sr}$, $(Z''_w)_{\rm sr}$ and the pre-shock value of $\hat{\phi}_{\hat{x}\hat{x}}$. The above results indicates that 3D (or unsteady) influence on the local structure of the pressure field can result only through changes in the *three* parameters, namely, $[\![\hat{u}]\!]_{\rm sr}$, $\hat{x}_{\rm sr}$ and x_1. A formal development for a small perturbation in $\hat{u}$ in these three parameters at a fixed $\hat{x}$ and $\hat{z}$ then yields from (2.31)

$$\frac{\delta\hat{u}}{|[\![\hat{u}_0]\!]_{\rm sr}|} \sim \mathscr{D}\ln|\zeta| + d + d_1\xi\ln|\zeta| + d_2\eta\arg(\zeta) + e\xi + e_1\eta + \ldots, \tag{2.32}$$

where $\mathscr{D}$, d, d_1, etc., are known functions of $[\![\hat{u}]\!]_{\rm sr}$, Z''_w and the perturbations of the three parameters mentioned. This can be matched with the logarithmically singular field of $\epsilon(\hat{\phi}_1)_x$, permitting the final determination of the corrected values of $[\![\hat{u}]\!]_{\rm sr}$, $\hat{x}_{\rm sr}$ and κ_1.

3. Outer solution and matching

3.1. *The outer solution*

In the flow domain of interest ($\Theta^2 < K_n = O(1)$) the basic outer flow is described by the linear, elliptic Prandtl–Glauert equation. For subsequent analysis, we shall employ a set of dimensionless variables

$$\bar{x} \equiv x/Bb, \quad \bar{y} \equiv y/b, \quad \bar{z} \equiv z/b, \quad \bar{\phi} \equiv 2\phi/\alpha_1^{\frac{2}{3}}U_\infty c_0, \tag{3.1}$$

with $B \equiv (1-M_\infty^2)^{\frac{1}{2}}$ and $\alpha_1 \equiv \alpha/M_\infty$, and assume an expansion for a dimensionless perturbation potential

$$\bar{\phi} = \bar{\phi}_0 + \epsilon\bar{\phi}_1 + \ldots, \tag{3.2}$$

where a weak (logarithmic) dependence of ϕ_1 on ϵ is anticipated. The term $\epsilon\bar{\phi}_1$ accounts for the higher aspect-ratio effect as well as the nonlinear correction to the outer solution. Partial differential equation (2.1) yields equations governing $\bar{\phi}_0, \bar{\phi}_1, \ldots$

$$\left.\begin{aligned}\left(\frac{\partial^2}{\partial\bar{x}^2} + \frac{\partial^2}{\partial\bar{y}^2} + \frac{\partial^2}{\partial\bar{z}^2}\right)\bar{\phi}_0 &= 0,\\ \left(\frac{\partial^2}{\partial\bar{x}^2} + \frac{\partial^2}{\partial\bar{y}^2} + \frac{\partial^2}{\partial\bar{z}^2}\right)\bar{\phi}_1 &= \frac{\gamma+1}{2K_0^{\frac{2}{3}}}\frac{\partial}{\partial\bar{x}}(\bar{\phi}_{0\bar{x}})^2.\end{aligned}\right\} \tag{3.3}$$

In the far field, the gradient of $\bar{\phi}_0$, $\bar{\phi}_1$, etc., are required to vanish, and on the wing trace behind the centre-line, the continuity of the pressure and normal velocity across the trailing-vortex sheet dictates that the partial $\bar{x}$ and $\bar{z}$ derivatives of $\bar{\phi}_0$ and $\bar{\phi}_1$ be continuous there.

The $\bar{\phi}_0$ is the velocity potential for a lifting line, representing the bound and trailing vortex system associated with the centre-line $x = x^c(y)$:

$$\bar{\phi}_0 = \frac{\bar{z}}{4\pi}\int_{-1}^{1} \frac{\bar{\Gamma}_0(y_1)}{(\bar{y}-\bar{y}_1)^2+\bar{z}^2}\left[1+\frac{\bar{x}-\bar{x}_c(\bar{y}_1)}{R_1}\right]d\bar{y}_1, \tag{3.4}$$

where $R_1 \equiv [(\bar{x}-\bar{x}_c(\bar{y}_1))^2+(\bar{y}-\bar{y}_1)^2+\bar{z}^2]^{\frac{1}{2}}$.

3.2. *The lifting-line solution in the inner limit*

In approaching the centre-line, i.e. $\bar{\xi} \equiv \bar{x}-\bar{x}_c(\bar{y}) \to 0$, $\hat{z} \to 0$, the integrand shown in (3.4) becomes nonintegrable at $\bar{y}_1 = \bar{y}$. By subtracting a suitable function, say g, from the integrand, the resultant integral may then yield a limit as $\bar{\xi}$ and $\bar{z}$ vanish. This, together with the quadrature of g, gives the behaviour of $\bar{\phi}_0$ in the inner limit sought. This procedure has been used in the analysis for straight oblique wings (Cheng 1978*a*, *b*). Among the indefinite integrals involved (described in more detail in Cheng & Meng 1979*b*), the following two are basic

$$\int \frac{du}{(u-i\bar{z})R} = \frac{1}{\zeta_0^{\frac{1}{2}}}\ln\left(\frac{\chi}{u-i\bar{z}}\right), \quad \int \frac{du}{R} = \ln|R+u+\bar{b}_0|, \tag{3.5}$$

where $\bar{b}_0\,(\neq b_0)$, $\bar{c}_0\,(\neq c_0)$, $\zeta_0^{\frac{1}{2}}$ and R are

$$\bar{b}_0 \equiv -\bar{m}\bar{\xi}/(1+\bar{m}^2), \quad \bar{c}_0 \equiv (\bar{\xi}^2+\bar{z}^2)/(1+\bar{m}^2), \quad \zeta_0^{\frac{1}{2}} \equiv (\bar{\xi}-i\bar{m}\bar{z})/(1+\bar{m}^2)^{\frac{1}{2}}, \tag{3.6a}$$

$$R \equiv (u^2+2\bar{b}_0u+\bar{c}_0)^{\frac{1}{2}}, \quad \chi \equiv P+iQ, \tag{3.6b}$$

with

$$P \equiv \bar{c}_0+\bar{b}_0u-\text{R.P.}\,\zeta_0^{\frac{1}{2}}R, \quad Q \equiv \bar{z}(\bar{b}_0+u)-\text{I.P.}\,\zeta_0^{\frac{1}{2}}R. \tag{3.6c}$$

The equation $\bar{x} = \bar{x}_c(\bar{y})$ defines the centre-line in the Prandtl–Glauert variables.

To arrive at a suitable form for matching with the inner solution, the result for small $\bar{\xi} = \bar{x}-\bar{x}_c(\bar{y})$ and $\bar{z}$ is first transformed to a system of curvilinear orthogonal co-ordinates $(\bar{x}', \bar{y}', \bar{z}')$, with $\bar{z}' = \bar{z}$, and the curved $\bar{y}'$ axis identified with $\bar{x} = \bar{x}_c(\bar{y})$. This is followed by a transformation to the inner variables $\hat{x}$, $\hat{z}$ and $\hat{y}$. The final result for $\bar{\phi}_0$ in the inner limit is

$$\bar{\phi}_0 \sim \frac{\bar{\Gamma}_0((\hat{y}))}{2\pi}\left[\tan^{-1}\left(\frac{\hat{x}}{K_n^{\frac{1}{2}}\hat{z}}\right)+\frac{\pi}{2}\operatorname{sgn}\hat{z}\right] + \epsilon\frac{\Theta}{K_n^{\frac{1}{2}}}\left(\frac{d}{d\hat{y}}+\frac{1}{2}\frac{K_0}{K_n}\frac{\Theta'}{\Theta}\right)\frac{\bar{\Gamma}_0}{2\pi}\hat{z}\,(\ln|\xi|-\ln 2)$$
$$+\epsilon\frac{\Theta^2\Theta'}{2K_n^{\frac{1}{2}}}\frac{\bar{\Gamma}_0}{2\pi}\frac{\hat{z}^3}{|\xi|^2}+\epsilon\,\bar{V}_1^{\infty}\hat{z}+\ldots, \tag{3.7a}$$

where the remainder is comparable to $\epsilon|\xi|^2$, $\bar{\Gamma}_0((\hat{y})) = \bar{\bar{\Gamma}}_0(\bar{y}') = \bar{\Gamma}_0(\bar{y})$, and

$$4\pi\bar{V}_1^{\infty} \equiv -\frac{\Theta^2\Theta'}{K_n^{\frac{3}{2}}}\bar{\Gamma}_0(\bar{y}) - \frac{1}{2\bar{\Gamma}_0(\bar{y})}\frac{d}{d\bar{y}}(\sin\bar{\Lambda}\bar{\Gamma}_0^2)\left[\ln\left|\frac{K_n}{\epsilon^2}\right|+\ln\left|\frac{1-\bar{y}^2}{\cos^2\bar{\Lambda}}\right|+2\right]$$
$$+2\bar{\Gamma}_0\frac{d\bar{\Lambda}}{d\bar{y}'}+\frac{d\bar{\Gamma}_0}{d\bar{y}}\ln\left|\frac{1-\bar{y}}{1+\bar{y}}\frac{1+\sin\bar{\Lambda}}{1-\sin\bar{\Lambda}}\right|+\int_{-1}^{1}\frac{\bar{\Gamma}_0'(\bar{y}_1)-\bar{\Gamma}_0'(\bar{y})}{\bar{y}_1-\bar{y}}[1-\sin\bar{\Lambda}\operatorname{sgn}(\bar{y}_1-\bar{y})]\,d\bar{y}_1$$

$$-\int_{-1}^{1}\frac{1}{(\bar{y}_1-\bar{y})^2}\left\{\bar{\Gamma}_0(\bar{y}_1)\left[\frac{\bar{x}_c(\bar{y}_1)-\bar{x}_c(\bar{y})}{\sqrt{(\bar{x}_c(\bar{y}_1)-\bar{x}_c(\bar{y}))^2+(\bar{y}_1-\bar{y})^2}}-\sin\bar{\Lambda}\,\mathrm{sgn}\,(\bar{y}_1-\bar{y})\right]\right.$$

$$\left.-\frac{1}{2}\frac{d\bar{\Lambda}}{d\bar{y}'}\,\bar{\Gamma}_0(\bar{y})\,|\bar{y}_1-\bar{y}|\right\}d\bar{y}_1, \tag{3.7b}$$

where $\cos\bar{\Lambda}=B\cos\Lambda(1-M_n^2)^{\frac{1}{2}}=(K_0/K_n)^{\frac{1}{2}}$, $\sin\bar{\Lambda}=\sin\Lambda/(1-M_n^2)^{\frac{1}{2}}=\Theta/K_n^{\frac{1}{2}}$,

$$\tan\bar{\Lambda}=\tan\Lambda/B,\quad d\bar{\Lambda}/d\bar{y}'=K_0K_n^{-\frac{3}{2}}\Theta'.$$

Note that $d\bar{y}'/d\bar{y}=\sec\bar{\Lambda}$, $K_0=K_n-\Theta^2$, and that we have replaced $\cos\Lambda$ (not $\cos\bar{\Lambda}$) by unity, and y by $\bar{y}$, throughout (3.7) except in the leading term (cf. § 2.1).†

The outer expansion of the inner solution $(\hat{\phi}_0+\epsilon\hat{\phi}_1+\ldots)$, according to (2.24) and (2.25), share a domain of validity with the inner expansion of the outer solution $(\bar{\phi}_0+\ldots)$ in $1\ll|\xi|\ll\epsilon^{-1}$ where matching is achieved after identifying

$$\left.\begin{aligned}&\bar{\Gamma}_0(\bar{y})\equiv\bar{\Gamma}_0((\hat{y}))=(\cos\Lambda)^{\frac{1}{2}}\hat{\Gamma}_0(\hat{y}),\quad \hat{\mathbb{C}}_0^r(\hat{y})=0,\\&\hat{\mathbb{C}}_1^i(\hat{y})=-(K_n)^{-\frac{1}{2}}[\bar{V}_1^\infty-(8\pi\bar{\Gamma}_0)^{-1}\ln 4\,\frac{d}{d\bar{y}}(\sin\bar{\Lambda}\bar{\Gamma}_0^2)].\end{aligned}\right\} \tag{3.8}$$

The induced upwash and, hence, the inner solution is completely determined. Terms in $(\hat{\phi}_0+\epsilon\hat{\phi}_1)$ not matched at this stage are those from the inner solutions belonging to order

$$|\xi|^{-1}\,|\ln\xi|,\quad |\xi|^{-1},\quad \epsilon\,|\ln\xi|^2,\quad \epsilon\,|\ln\xi|,\quad \epsilon. \tag{3.9}$$

These should find their counterparts in $\bar{\phi}_1$ which includes the nonlinear corrections to the outer solution.

The upwash function $\bar{V}_1^\infty$ is dominated by a logarithmically large term

$$-\frac{1}{8\pi\bar{\Gamma}_0}\frac{d}{d\bar{y}}(\sin\bar{\Lambda}\,\bar{\Gamma}_0^2)\ln\left|\frac{K_0}{\epsilon^2}\right|=-\frac{1}{4\pi}\left[\sin\bar{\Lambda}\frac{d\bar{\Gamma}_0}{dy}+\tfrac{1}{2}\cos\bar{\Lambda}\frac{d\bar{\Lambda}}{dy}\,\bar{\Gamma}_0\right]\ln\left|\frac{K_0}{\epsilon^2}\right|, \tag{3.10}$$

the part proportional to $d\bar{\Gamma}_0/d\bar{y}$ represents the important influence of the near wake, the part proportional $\bar{\Gamma}_0 d\bar{\Lambda}/d\bar{y}$ gives the self induced velocity of the bound vortices. These, together with other competing contributions, lead generally to a maximum induced upwash near the tip on the aft wing panel and a maximum induced downwash near the tip on a swept-forward panel, as noted earlier by Cheng (1978*b*, p. 17).

In the very special limit corresponding to an unyawed straight wing ($\Theta\to 0$), the upwash correction determined from (3.7*a*) and (3.7*b*) agrees with the linear subsonic results of Jones & Cohen (1957). Interestingly, for a symmetric swept wing, i.e. $\bar{x}_c(\bar{y})=m|\bar{y}|$, the last integral of $\bar{V}_1^\infty$ diverges in approaching the wing apex like

$$\bar{V}_1^\infty\sim-\bar{\Gamma}_0(0)\frac{\sin\bar{\Lambda}}{4\pi\bar{y}}. \tag{3.11}$$

This agrees with the downwash induced by the bound vortices on the opposite wing panel computed according to the Biot–Savart law. It exhibits clearly a non-uniformity at $\bar{y}=O(\epsilon)$.

We point out in passing that the outer solution involving the higher-order coefficient, $\bar{\phi}_1$, has been studied in the inner limit in Cheng & Meng (1979*b*) for a straight oblique

† For oblique wings ($\Theta'=0$), $\bar{V}_1^\infty$ is precisely the $\bar{\Sigma}$ in Cheng & Meng (1979*a*, *b*).

wing, where matching with the inner solution, including all terms shown in (2.24), (2.25) and (2.26), has been demonstrated.

4. Straight oblique wings

For applications to the type of oblique wings considered by Jones (1971, 1977), the centre-line can be assumed to be straight, i.e. $\Theta' \equiv 0$, p.d.e. (2.5) reduces to

$$\frac{\partial}{\partial \hat{x}}\left[K_n \hat{\phi}_{\hat{x}} - \frac{\gamma+1}{2}\hat{\phi}_{\hat{x}}^2\right] + \hat{\phi}_{\hat{z}\hat{z}} = 2\epsilon\Theta\hat{\phi}_{\hat{x}\hat{y}} + \ldots \tag{4.1}$$

subject to errors of $O(\epsilon^2)$. If $\hat{y}$ is taken as a normalized time variable, (4.1) can be interpreted as one governing a 2D transonic small-disturbance flow *near* the quasi-steady limit, in which the RHS represents an unsteady correction. The perturbation solution $(\hat{\phi}_0 + \epsilon\hat{\phi}_1 + \ldots)$ under $\Theta' \equiv 0$ also admits a local-similarity in $\hat{\phi}_0$ and in $\hat{\phi}_1$, applicable to a rather useful class of wing geometry; the reduced problems in this case can be solved *once* for *all* span stations. These will be discussed in §§ 4.1 and 4.2 below.

4.1. *An unsteady analogy with a 2D transonic flow*

To bring out more precisely the nature of the analogy in question, we introduce

$$\varphi \equiv \hat{\phi} + \epsilon K_n^{\frac{1}{2}} \hat{\mathbb{C}}_1^i \hat{z}, \quad \hat{t} \equiv \hat{y}/\epsilon\Theta. \tag{4.2}$$

p.d.e. (4.1) then takes the form

$$\frac{\partial}{\partial \hat{x}}\left[K_n \varphi_{\hat{x}} - \frac{\gamma+1}{2}\varphi_{\hat{x}}^2\right] + \varphi_{\hat{z}\hat{z}} = 2\varphi_{\hat{x}\hat{t}}, \tag{4.3}$$

familiar in most nonlinear analysis of unsteady transonic flows (Landahl 1962; Oswatitsch 1962; Timman 1962). The equations for the characteristics and the shock relations, (2.10) and (2.13), also go over correctly, upon substituting (4.2), to the unsteady transonic system in question, and the continuity requirements on $\hat{\phi}_{\hat{x}}$ and $\hat{\phi}_{\hat{z}}$, (2.9), remain unchanged. The wing boundary condition (2.8) becomes

$$\left(\frac{\partial \varphi}{\partial \hat{z}}\right)_w \equiv \frac{\partial}{\partial \hat{x}}\hat{Z}^{\pm} + \frac{d}{d\hat{t}}\hat{Z}_B + \epsilon(\hat{l} + K_n^{\frac{1}{2}}\hat{\mathbb{C}}_1^i). \tag{4.4}$$

The far-field description for $\varphi = \hat{\phi}_0 + \epsilon\hat{\phi}_1 + \epsilon K_n^{\frac{1}{2}}\hat{\mathbb{C}}_1^i\hat{z}$ based on the expressions for $\hat{\phi}_0$ and $\hat{\phi}_1$ of (2.24) and (2.25), with $\partial/\partial\hat{t}$ replacing $\epsilon\Theta\,\partial/\partial\hat{y}$ and $\Theta' \equiv 0$ is precisely that describing the solution to (4.3) at large $|\xi|$ near the quasi-steady limit. One must note that the induced-upwash term $\epsilon K_n^{\frac{1}{2}}\hat{\mathbb{C}}_1^i\hat{z}$ in φ, (4.2), cancels out the corresponding term in $\epsilon\hat{\phi}_1$ from (2.25), and therefore the resultant far-field description for φ is independent of the influence of the far-wake vorticity. Hence, our *inner* airfoil problem is mathematically equivalent to that of a (special) unsteady transonic airfoil pertaining to the nonlinear (lower-frequency) domain governed by p.d.e. (4.3) *near* the *quasi-steady* limit, with a wing-surface condition (4.4), and time-dependent locations of the leading and trailing edges. The far-wake influence of the oblique-wing, as well as the wing bend and wing twist, thus appear as additional incidence corrections in the equivalent unsteady problem.

The foregoing examination indicates that the solution to the oblique-wing problem can be generated from an unsteady 2D calculation based on (4.3), for which existing numerical procedure, for example, those using alternating direction implicit algorithms similar to Ballhaus & Goorjian (1977), can be adapted. The crucial input to such an application lies, of course, in the incidence correction. To utilize fully the (available) computer storage and time for the analysis, the description for φ based on (2.24) and (2.25) should be used at the far boundary. (The values of $\hat{\Gamma}_0^r$, $\hat{D}_0^i$ and $\hat{D}_0^r$ in (2.25) can be taken from those determined from the previous time step or from a rough integration of (4.3) and (4.4) with $\mathbb{C}_1^i = 0$.)

The approach via this unsteady analogy promises an alternative solution procedure without the requirement for the local similarity (cf. (4.5) below) as well as providing a method for capturing shock waves on oblique wings without the difficulty associated with the re-expansion singularity discussed earlier (§ 2.4). Sample calculations via the unsteady analogy and their comparison with the perturbation solutions have been given in Cheng & Meng (1979*b*) for a subcritical case.† From the viewpoint of unsteady transonic-flow analysis, it is of interest to point out that the treatment of the non-uniformity at the shock root described in § 2.3 applies equally well to the corresponding problem arising from the unsteady perturbation considered by Ehlers (1974), Traci, Albano & Farr (1976), Hafez, Rizk & Murman (1977) and Fung, Yu & Seebass (1978).

4.2. *Local similarities*

Owing to the linearity, the 3D correction to $\hat{\phi}$, $\epsilon\hat{\phi}_1$, can be decomposed into suitably scaled separate parts. For a certain class of oblique-wing geometry, these separate parts have similarity solutions independent of $\hat{y}$, as does the basic solution $\hat{\phi}_0$. This wing class requires, in addition to $\Theta' \equiv 0$, or $|\Theta'| \ll 1$, that the basic wing section at each span station be generated from a single airfoil shape of the same thickness ratio at a fixed incidence. More specifically, it requires a form of wing co-ordinates

$$z' = \frac{c_0}{2}\left[\hat{c}(\hat{y})\alpha\bar{Z}^{\pm}\left(\frac{\hat{x}}{\hat{c}}\right) + \alpha^{\frac{1}{3}}\hat{Z}_B(\hat{y}) + \alpha\epsilon(\hat{x}-\hat{x}_0)\,\hat{I}(\hat{y})\right], \tag{4.5}$$

where $\hat{c}(\hat{y})$ is the ratio of the local wing chord $c(\hat{y})$ to the root chord c_0. Implicit is that $\hat{x} = 0$ is a straight axis on the wing; the planform, as well as the functions $\hat{Z}_B(y)$ and $I(y)$, are otherwise quite arbitrary.

For this case, we introduce the variables (with $b' = \sec\Lambda b$)

$$\tilde{x} \equiv \hat{x}/\hat{c} = 2x'/c(\hat{y}), \quad \tilde{z} \equiv \tilde{z}/\hat{c} = 2\alpha^{\frac{1}{3}}z'/c(\hat{y}), \quad \tilde{y} \equiv \cos\Lambda\hat{y} = y'/b', \tag{4.6}$$

and assume

$$\hat{\phi}/\hat{c} = \tilde{\phi}_0 + \epsilon\Theta\hat{c}'\tilde{\phi}_1 + \epsilon[K_n^{\frac{1}{3}}\tilde{\mathbb{C}}_1^i(\tilde{y}) + \hat{I}(\tilde{y}) + \Theta\hat{Z}_B'(\tilde{y})]\,\tilde{\phi}_2 - \epsilon K_n^{\frac{1}{3}}\tilde{\mathbb{C}}_1^i\tilde{z} + \ldots, \tag{4.7}$$

where $\tilde{\phi}_0$, $\tilde{\phi}_1$, and $\tilde{\phi}_z$ are independent of $\tilde{y}$, and $\hat{c}' \equiv d\hat{c}/d\tilde{y}$. The separation into $\tilde{\phi}_1$ and

† The unsteady solutions were obtained by Dr T. Evans, University of East Anglia, using a procedure similar to that of Ballhaus & Goorjian (1977). With the inclusion of $\epsilon\Theta'\psi_z$ on the right-hand side of (4.3), the unsteady analogy can be used as a procedure for solving p.d.e. (2.6) with a non-vanishing centre-line curvature.

ϕ_2 allows the induced-upwash effect to be treated independently of the spanwise-compressibility correction. The p.d.e. (2.16) and (2.18) become in this case

$$\frac{\partial}{\partial\tilde{x}}\left[K_n\phi_{0\tilde{x}}-\frac{\gamma+1}{2}(\phi_{0\tilde{x}})^2\right]+\frac{\partial^2}{\partial\tilde{z}^2}\phi_0=0, \tag{4.8a}$$

$$\left\{[K_n-(\gamma+1)\phi_{0\tilde{x}}]\frac{\partial^2}{\partial\tilde{x}^2}+\frac{\partial^2}{\partial\tilde{z}^2}-(\gamma+1)\phi_{0\tilde{x}\tilde{x}}\frac{\partial}{\partial\tilde{x}}\right\}\phi_1=-2\left(\tilde{x}\frac{\partial}{\partial\tilde{x}}+\tilde{z}\frac{\partial}{\partial\tilde{z}}\right)\phi_{0\tilde{x}}, \tag{4.8b}$$

$$\left\{[K_n-(\gamma+1)\phi_{0\tilde{x}}]\frac{\partial^2}{\partial\tilde{x}^2}+\frac{\partial^2}{\partial\tilde{z}^2}-(\gamma+1)\phi_{0\tilde{x}\tilde{x}}\frac{\partial}{\partial\tilde{x}}\right\}\phi_2=0. \tag{4.8c}$$

The right-hand member of (4.8*b*) arises from $\partial/\partial\hat{y}=\partial/\partial\tilde{y}-(\tilde{c}/\hat{c})(\tilde{x}\,\partial/\partial\tilde{x}+\tilde{z}\,\partial/\partial\tilde{z})$. The conditions on wing surfaces and the wake, (2.17) and (2.19), give

$$\left(\frac{\partial}{\partial\tilde{z}}\phi_0\right)_w=\frac{\partial}{\partial\tilde{x}}\tilde{Z}^{\pm},\quad\left(\frac{\partial}{\partial\tilde{z}}\phi_1\right)_w=0,\quad\left(\frac{\partial}{\partial\tilde{z}}\phi_2\right)_w=1; \tag{4.9a, b, c}$$

and

$$[\![\phi_{0\tilde{x}}]\!]_{\mathrm{TV}}=[\![\phi_{0\tilde{z}}]\!]_{\mathrm{TV}}=0,\quad[\![\phi_{1\tilde{x}}]\!]_{\mathrm{TV}}=[\![\phi_{1\tilde{z}}]\!]_{\mathrm{TV}}=0,\quad[\![\phi_{2\tilde{x}}]\!]_{\mathrm{TV}}=[\![\phi_{2\tilde{z}}]\!]_{\mathrm{TV}}=0. \tag{4.10a, b, c}$$

Consistent with the similarity structure of $\hat{\phi}/\hat{c}$, (4.7), the equation of the shock boundary (2.21) takes the form

$$\hat{x}/\hat{c}=\tilde{x}_0^D(\tilde{z})+\epsilon\Theta\hat{c}'(\hat{y})\,\tilde{x}_1^D(\tilde{z})+\epsilon[K_n^{\frac{1}{2}}\tilde{\mathbb{C}}_1^i(\tilde{y})+\hat{I}(\tilde{y})+\Theta\hat{Z}_B']\,\tilde{x}_2^D(\tilde{z}). \tag{4.11}$$

The shock relations transferred to the unperturbed shock boundary, i.e. (2.22) and (2.23), now read as, at $\tilde{x}=\tilde{x}_0^D(\tilde{z})$,†

$$K_n-(\gamma+1)\langle\phi_{0\tilde{x}}\rangle=-(\partial\tilde{x}_0^D/\partial\tilde{z})^2, \tag{4.12a}$$

$$2\tilde{x}_0^D-(\gamma+1)\langle\phi_{1\tilde{x}}+\tilde{x}_1^D\phi_{0\tilde{x}\tilde{x}}\rangle=-2(\partial\tilde{x}_0^D/\partial\tilde{z})(\partial\tilde{x}_1^D/\partial\tilde{z}), \tag{4.12b}$$

$$-(\gamma+1)\langle\phi_{2\tilde{x}}+\tilde{x}_2^D\phi_{0\tilde{x}\tilde{x}}\rangle=-2(\partial\tilde{x}_0^D/\partial\tilde{z})(\partial\tilde{x}_2^D/\partial\tilde{z}) \tag{4.12c}$$

$$[\![\phi_0]\!]=[\![\phi_1+\tilde{x}_1^D\phi_{0\tilde{x}}]\!]=[\![\phi_2+\tilde{x}_2^D\phi_{0\tilde{x}}]\!]=0. \tag{4.13a, b, c}$$

Approaching the outer limit, $|\tilde{\zeta}|=|\zeta/\hat{c}|\to\infty$, p.d.e. (4.8*a*, *b*) admits the developments

$$\phi_0\sim\frac{\tilde{\Gamma}_0}{2\pi}\left[\tan^{-1}\left(\frac{\tilde{x}}{K_n^{\frac{1}{2}}\tilde{z}}\right)+\frac{\pi}{2}\operatorname{sgn}\tilde{z}\right]+(\tilde{D}_0^r\tilde{x}+\tilde{D}_0^iK_n^{\frac{1}{2}}\tilde{z})/|\tilde{\zeta}|^2$$
$$+\frac{\gamma+1}{4K_n}\left(\frac{\tilde{\Gamma}_0}{2\pi}\right)^2[\ln|\tilde{\zeta}|+K_n\tilde{z}^2/|\tilde{\zeta}|^2]\,\tilde{x}/|\tilde{\zeta}|^2+\ldots, \tag{4.14a}$$

$$\phi_1\sim\frac{\tilde{z}}{K_n^{\frac{1}{2}}}\frac{\tilde{\Gamma}_0}{2\pi}\ln|\tilde{\zeta}|+\frac{\gamma+1}{32K_n^2}\left(\frac{\tilde{\Gamma}_0}{\pi}\right)^2\left\{2(\ln|\tilde{\zeta}|)^2+2\frac{\tilde{x}^2-K_n\tilde{z}^2}{|\tilde{\zeta}|^2}\ln|\tilde{\zeta}|\right.$$
$$\left.-\tfrac{1}{2}[(\tilde{x}^2-K_n\tilde{z}^2)^2-4K_n\tilde{z}^2\tilde{x}^2]/|\tilde{\zeta}|^2\right\}+\frac{\tilde{Q}_1}{2\pi}\ln|\tilde{\zeta}|+\frac{\tilde{\Gamma}_1}{2\pi}\left[\tan^{-1}\left(\frac{\tilde{x}}{K_n^{\frac{1}{2}}\tilde{z}}\right)+\frac{\pi}{2}\operatorname{sgn}\tilde{z}\right]$$
$$+\frac{2}{K_n^{\frac{1}{2}}}(\tilde{D}_0^i\tilde{x}-\tilde{D}_0^rK_n^{\frac{1}{2}}\tilde{z})\tilde{z}/|\tilde{\zeta}|^2+\ldots, \tag{4.14b}$$

† These jump conditions for ϕ_1 and ϕ_2 are not the same as those for the (formal) weak solutions of p.d.e. (4.8*b*) and (4.8*c*).

$$\phi_2 \sim \frac{\tilde{\Gamma}_2}{2\pi}\left[\tan^{-1}\left(\frac{\tilde{x}}{\sqrt{(K_n)}\tilde{z}}\right)+\frac{\pi}{2}\operatorname{sgn}\tilde{z}\right]+(\gamma+1)\,8^{-1}\pi^{-2}K_n^{-2}\tilde{\Gamma}_0\tilde{\Gamma}_2[\ln|\tilde{\zeta}| + K_n\tilde{z}^2/|\tilde{\zeta}|^2]\,\tilde{x}/|\tilde{\zeta}|^2+(\tilde{D}_2^r\tilde{x}+\tilde{D}_2^i\tilde{z})/|\tilde{\zeta}|^2+\dots. \quad (4.14c)$$

These results are recoverable (completely) from the far-field expansion for

$$\hat{\phi} = \hat{\phi}_0+\epsilon\hat{\phi}_1+\dots$$

in the more general case, (2.24) and (2.25), through transformations (4.6) and (4.7) and the relations for the coefficients

$$\tilde{\Gamma}_0 = \hat{\Gamma}_0/\hat{c}, \quad \tilde{D}_0^i = \hat{D}_0^i/\hat{c}^2, \quad \tilde{D}_0^r = \hat{D}_0^r/\hat{c}^2+\frac{\gamma+1}{16K_n}\left(\frac{\hat{\Gamma}_0}{\pi\hat{c}}\right)^2\ln\hat{c}; \quad (4.15)$$

$$\tilde{\mathbb{C}}_1^i = \hat{\mathbb{C}}_1^i-\frac{\Theta}{2K_n}\left(\frac{\hat{\Gamma}_0}{\pi\hat{c}}\right)\hat{c}'\ln\hat{c}, \quad (4.16a)$$

$$\tilde{Q}_1 = \frac{\hat{Q}_1}{\Theta\hat{c}\hat{c}'}+\frac{\gamma+1}{4\pi K_n^2}\left(\frac{\hat{\Gamma}_0}{\hat{c}}\right)^2\ln\hat{c}, \quad (4.16b)$$

$$\hat{\Gamma}_1 = \Theta\hat{c}\hat{c}'\tilde{\Gamma}_1+[K_n^{\frac{1}{2}}+\tilde{\mathbb{C}}_1^i+\hat{I}+\Theta\hat{Z}_B']\,\tilde{\Gamma}_2. \quad (4.16c)$$

We note that, according to the last of (4.15),

$$\frac{1}{2\hat{c}\hat{c}'}\frac{d}{d\hat{y}}\hat{D}_0^r = \tilde{D}_0^r-\frac{\gamma+1}{16K_n}\left(\frac{\tilde{\Gamma}_0}{\pi}\right)^2(\ln\hat{c}+\tfrac{1}{2}).$$

The $\frac{1}{2}$ in $(\ln\hat{c}+\frac{1}{2})$ above explains the formal difference of $(\ln|\tilde{\zeta}|+\frac{1}{2})$ in (2.26) and $\ln|\tilde{\zeta}|$ in the second term inside the curly bracket in (4.14*b*).

The source strength $\tilde{Q}_1$ can be explicitly evaluated in terms of $\tilde{D}_0^r$ and $\tilde{\Gamma}_0^2$ in this case with the help of the Green theorem, unaffected by the presence of imbedded shocks,

$$\tilde{Q}_1 = \frac{4\pi}{K_n}\tilde{D}_0^r+\frac{\gamma+1}{8\pi K_n^2}(\tilde{\Gamma}_0)^2[3+\tilde{a}+(\tilde{a}+\tilde{b})^2], \quad (4.17)$$

where $\tilde{a} = \hat{a}/\hat{c}$ and $\tilde{b} = \hat{b}/\hat{c} = 2+\tilde{a}$ are the leading and trailing-edge locations in $\tilde{x}$, respectively. Appendix III in Cheng & Meng (1979*b*) gives details of the derivation.

With $\tilde{\mathbb{C}}_1^i$ known, ways to control the induced upwash by wing twist and wing bend through (4.7) are evident. From the form of solution (4.7) the similitude of the 3D flow structure is also apparent.

5. Examples and discussion

Demonstration of solutions to the reduced problem is considered essential for the present study, inasmuch as their existence and uniqueness have not been thoroughly investigated. The present work is limited by the assumptions of a high aspect ratio and of the small disturbance; it is not at all apparent that the theory may adequately predict the inviscid aerodynamic characteristics to a degree enjoyed by the classical lifting-line theory. In addition, the possibility of committing algebraic errors in the present work is not necessarily low. Thus a direct comparison with 3D solutions obtained from a more exact full-potential equation is considered an important part of the present study.

5.1. *Procedure of computation: examples of similarity solutions*

Line-relaxation methods are used to solve the algebraic systems of the difference equations for the similarity solutions $\check{\phi}_0$, $\check{\phi}_1$, and $\check{\phi}_2$; the methods employ Murman's type-sensitive difference operators, including a shock-point operator (Murman & Cole 1971, Murman 1974). The basic computer code for $\check{\phi}_0$ is adopted from one used earlier in Hafez & Cheng's (1977*a*, *b*) studies, improved in the far-field description with (4.14*a*) and in the use of a higher-order convergence acceleration scheme. The doublet strength $\tilde{D}_0^r$ and $\tilde{D}_0^i$ in (4.14*a*) are determined by a least-square fit of data *near and at* the far boundary. The inclusion of the doublets and the nonlinear terms shown in (4.14*a*) have improved substantially the accuracy and internal consistency of the numerical solutions at the far boundary. The basic program will also furnish input data for the relaxation solutions using shock-fitting algorithms (Hafez & Cheng 1977*b*) which was not needed, however, in the shock-free examples considered below.

The procedures for $\check{\phi}_1$ and $\check{\phi}_2$ solving the linear p.d.e.'s, with conditions on the x axis and the far-field description, (4.8)–(4.17), are similar to that for $\check{\phi}_0$. The programs are simpler in that the transition boundary is fixed to the sonic boundary for $\check{\phi}_0$, but it requires a larger storage for the inclusion of $\check{\phi}_0$ in addition to the $\check{\phi}_1$'s obtained in previous iterations. The same grid with non-uniform mesh is employed for $\check{\phi}_0$, $\check{\phi}_1$, and $\check{\phi}_2$, covering a region $|\tilde{x}| \leqslant 6$, $|\tilde{z}| \leqslant 6$, with a total of 81×65 grid points. The leading edge is made to locate at $\tilde{x} = -1$, and the trailing edge at $\tilde{x} = 1$ (i.e. $\tilde{a} = -1$, $\tilde{b} = 1$), any departure of $\tilde{a}$ from -1 is accounted for by changing $\tilde{x}$ into $[\tilde{x} + (1 + \tilde{a})]$ in (4.8) through (4.17). The case $|\tilde{x}| = 1$ corresponds to an oblique-wing planform with fore-and-aft symmetry about the (straight) centre-line. The Kutta condition is implicit in the programs in requiring the continuity of $\check{\phi}_{0\tilde{x}}$, $\check{\phi}_{1\tilde{x}}$ and $\check{\phi}_{2\tilde{x}}$ at the trailing edge.

The iterative solutions use a relaxation factor 1·8 in the elliptic region and 0·8 in the hyperbolic region; typically 200 line-sweeps are needed for the convergence of the circulations to within 10^{-5}. The calculation for $\check{\phi}_1$ involves more work, and requires fifteen (15) minutes on an IBM 3031, using double-precision arithmetic.

As examples, we apply the solution procedure to oblique wings with the section function $\tilde{z}^{\pm}(x)$ generated from the N.A.S.A. 3612-02, 40 airfoil, scaled to an arbitrary thickness. For the present purpose, we assume that the straight axis ($\tilde{x} = 0$) coincides with the mid chord of each wing section; the spanwise distribution of the wing chord is, however, left arbitrary. In this application, it suffices to set the thickness-to-camber ratio τ/α equal to unity, thus, replacing all α by τ in the scales entering the definitions of $\tilde{z}$ and $\check{\phi}$, as well as K_n, Θ and ϵ. The determination of $\check{\phi}_0$, $\check{\phi}_1$, and $\check{\phi}_2$ requires the specification of the component similarity parameter K_n.

Figure 3 presents computed surface distributions of $\check{\phi}_{0\tilde{x}}$ (thin solid curves), $\check{\phi}_{1\tilde{x}}$ (heavy solid curves), and $\check{\phi}_{2\tilde{x}}$ (dash curves) for $K_n = 3{\cdot}6$. The 'u' and 'l' refer to the upper and the lower surfaces. The peak of $(\check{\phi}_0)_{\tilde{x}}$ occurs near the mid-cord point and lies slightly below the critical value $K_n/(\gamma + 1) = 1{\cdot}50$. The surface values of $(\check{\phi}_1)_{\tilde{x}}$ which arise from the spanwise variation of the compressibility correction are seen to be numerically small as compared to $(\check{\phi}_2)_{\tilde{x}}$. The latter accounts for the incidence correction and includes the far-wake vorticity influence. The circulations given by the jump of $\check{\phi}_0$, $\check{\phi}_1$, and $\check{\phi}_2$ at the trailing edge are found to be $\tilde{\Gamma}_0 = 2{\cdot}048$, $\tilde{\Gamma}_1 = -0{\cdot}494$, and $\tilde{\Gamma}_2 = -2{\cdot}667$, respectively. Their contributions to the potential $\hat{\phi}$ at the trailing edge, hence, the rolling moment about the wind axis, are weighted by $\hat{c}$, $\epsilon\Theta\hat{c}\, d\hat{c}/d\bar{y}$,

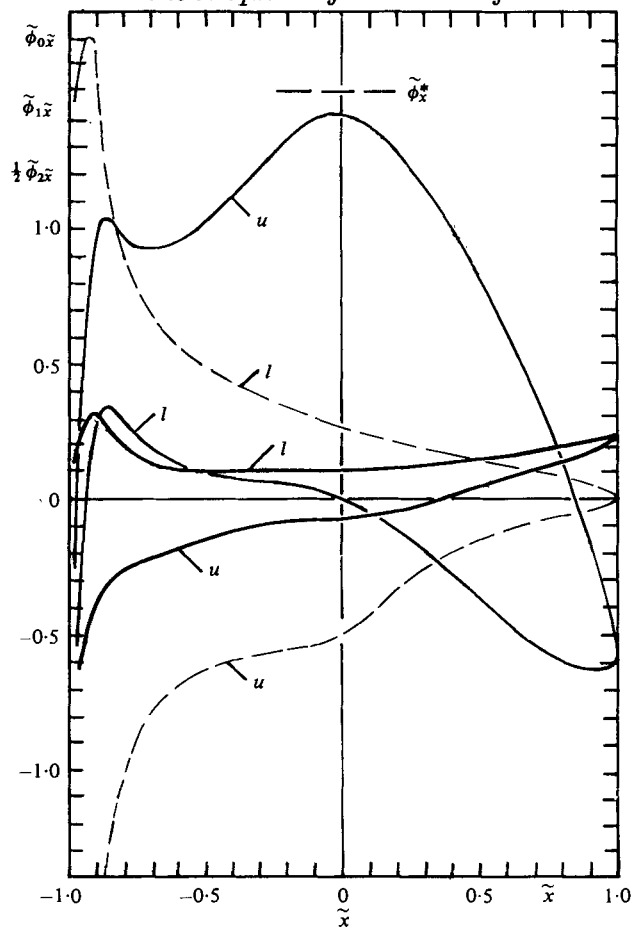

FIGURE 3. Examples of $\tilde{\phi}_{0\tilde{x}}$ (——), $\tilde{\phi}_{1\tilde{x}}$ (——), and $\tilde{\phi}_{2\tilde{x}}$ (– – –) on the upper and lower surfaces of a straight oblique wing at $K_n = 3{\cdot}6$. The airfoil section is N.A.S.A. 3612-02, 40 rescaled to an arbitrary thickness; wing has no twist and bend; local incidence is zero.

and $\epsilon\hat{c}[K_n^{\frac{1}{2}}\tilde{\mathbb{C}}_1^i + \tilde{I} + \Theta\hat{Z}'_B]$, respectively. For a planform which is symmetrical with respect to $\tilde{y} = 0$ (not $\bar{y} = 0$), $\hat{\mathbb{\Gamma}}_0$ is also symmetric. The induced upwash in this case is positive ($\mathbb{C}_1^i < 0$) on an aft panel and negative ($\tilde{\mathbb{C}}_1^i > 0$) on a fore panel, as noted earlier. Therefore, the last two of the three weighting factors mentioned are *both* negative on an aft panel and positive on a fore panel. It is, thus, seen from this example that, with the negative $\tilde{\mathbb{\Gamma}}_1$ and $\tilde{\mathbb{\Gamma}}_2$, the inviscid 3D effects will give rise to an unbalanced rolling moment (as well as pitching moment). The asymmetrical forces, if unchecked, will tend to raise the aft panel and lower the fore panel.

The least-square fit of the doublet strengths determined from the relaxation solution $\tilde{\phi}_0$ of figure 3 are $\tilde{D}_0^r = 0{\cdot}2472$ and $\tilde{D}_0^i = 0{\cdot}0958$; with these and the value of $\tilde{\mathbb{\Gamma}}_0 = 2{\cdot}048$, the source strength in the far field for $\tilde{\phi}_1$ is determined from (4.17) as $\tilde{Q}_1 = 0{\cdot}9270$. We note in passing that the program for computing $\tilde{\phi}_1$ is relatively straightforward and the result can be reproduced quite well by computing $\tilde{\phi}_0$ at a slightly different incidence, taking the difference of the two $\tilde{\phi}_0$'s, and normalizing.

Similar computations have been performed for other values of K_n, and other airfoil sections, including cases with slightly supercritical (2D) component flows.

5.2. *Elliptic planform: comparison with full-potential solutions*

Numerical results from the full-potential equation corresponding to cases analysed are generated from one version of A. Jameson's 3D codes 'FLO 22' (Jameson 1974, Jameson & Caughey 1977), which was applied with suitable implementations for oblique-wing analyses at N.A.S.A. Ames Research Centre, and at Grumman Aerospace Corporation Research Department. We point out that the FLO 22 data from Ames and from Grumman are not identical owing mainly to the use of different meshes. The availability of data from two sources is helpful in delineating the nature of any discrepancy between our theory and the more exact 3D program. Data from the latter is still influenced by the mesh size, spacing of the span stations, number of iterations, and the detail description of the leading-edge geometry.

A number of FLO 22 runs have been made with free-stream Mach number, swept angle, wing-thickness, etc., chosen to give the proper value of K_n, employing the same basic airfoil section (N.A.S.A. 3612-02,40). A symmetric elliptic planform is used in each case; wing twist and wing bend are assumed to be zero. Comparisons with those based on the similarity solutions has been made in a number of cases (Cheng & Meng 1979*b*). The comparison shown in figure 4 may be considered as being typical among most cases involving high subcritical and slightly supercritical component flows.

The oblique elliptic wing considered in figure 4 has a 6% thickness ratio, with the major-to-minor axes ratio of 20, and a sweep angle of 22·5°. The free-stream Mach number is $M_\infty = 0{\cdot}8242$, which makes $M_n = 0{\cdot}7615$ and $K_n = 3{\cdot}60$, $\Theta = 1{\cdot}003$ and $\epsilon = 0{\cdot}1277$ in the analysis of § 4.† The pressure coefficient $c_p \equiv (p-p_\infty)/\frac{1}{2}\rho_\infty U_\infty^2$ may therefore be computed from

$$C_p = \cos^2\Lambda c_p' = -2\cos^2\Lambda(\alpha/M_n)^{\frac{2}{3}}\left\{(\hat{\phi}_0)_{\bar{x}} + \epsilon\Theta\frac{d\hat{c}}{d\hat{y}}(\phi_1)_{\bar{x}} + \epsilon[K_n^{\frac{1}{2}}\tilde{C}_1^i(\tilde{y}) + \bar{I} + \Theta\bar{Z}_B'](\hat{\phi}_2)_{\bar{x}}\right\} \tag{5.1}$$

with data from figure 3. The critical C_p value where the (2D) *component* flow becomes sonic is $C_p^{**} = -0{\cdot}470$ in this case.‡ The surface C_p values at three span stations, $\tilde{y} = -0{\cdot}69$, $\tilde{y} = 0$, and $\tilde{y} = 0{\cdot}69$ are shown in figures 4 (*a*, *b*, *c*), respectively. The FLO 22 data from Ames (in small crosses and '$\vee$') and from Grumman (in small circles) are seen to be quite close except near the leading edge. In approaching the latter, the small-disturbance assumption of our theory also breaks down. The agreement of the FLO 22 data with our values computed on the basis of data from figure 3 (in solid curves) must be considered as being better than anticipated, inasmuch as the relative error in our theory is of an order determined by the larger of $\tau^{\frac{2}{3}}$ and ϵ^2 (to be precise). In the present case, $\tau^{\frac{2}{3}} = (0{\cdot}06)^{\frac{2}{3}} = 0{\cdot}153$!

Encouraging is that the degree of agreement with the FLO 22 data appear to deteriorate little with increasing wing-thickness ratio or reducing aspect ratio.

† The value of ϵ for figures 4 and 5 were computed with AR_0 taken as $AR_1 = AR_0\cos\Lambda$ which is permissible under the present theory [cf. remarks below (3.7*b*)].

‡ $c_p^{**} = -2\gamma^{-1}M_n^{-2}\left\{[(\gamma+1)/2(1+\frac{\gamma-1}{2}M_n^2)]^{-\gamma/(\gamma-1)}-1\right\}\cos^2\Lambda \simeq -2(\alpha/M_n)^{\frac{2}{3}}\cos^2\Lambda K_n/(\gamma+1)$.

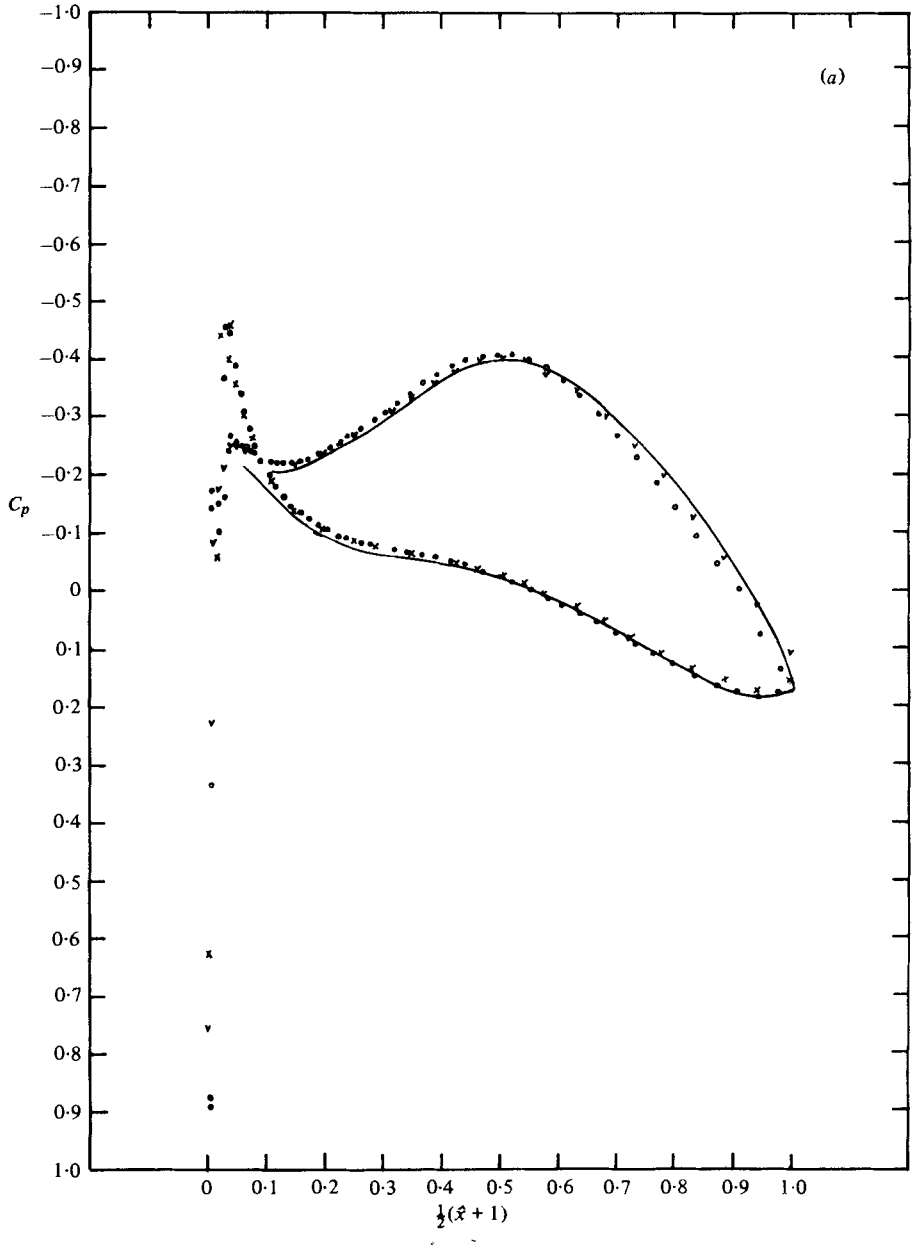

FIGURE 4(*a*). For legend see p. 551.

Figure 5 shows a typical comparison for elliptic wings with a thicker (12%) airfoil section and a lower aspect ratio (major-to-minor axes ratio of 14). The case considered has a free-stream Mach number 0·7677, a yaw angle 30°. This gives $M_n = 0{\cdot}6648$, $K_n = 3{\cdot}45$, $\epsilon = 0{\cdot}1448$, and $\Theta = 1{\cdot}062$; also $c_p^{**} = -0{\cdot}689$. The c_p values were computed from the present theory using data obtained for $\tilde{\phi}_{0\tilde{x}}$, etc. at $K_n = 3{\cdot}40$ similar to those shown in figure 3. To conserve space, only the comparison made at the span station $\tilde{y} = 0{\cdot}8$ is shown. The present results are shown in heavy curves with

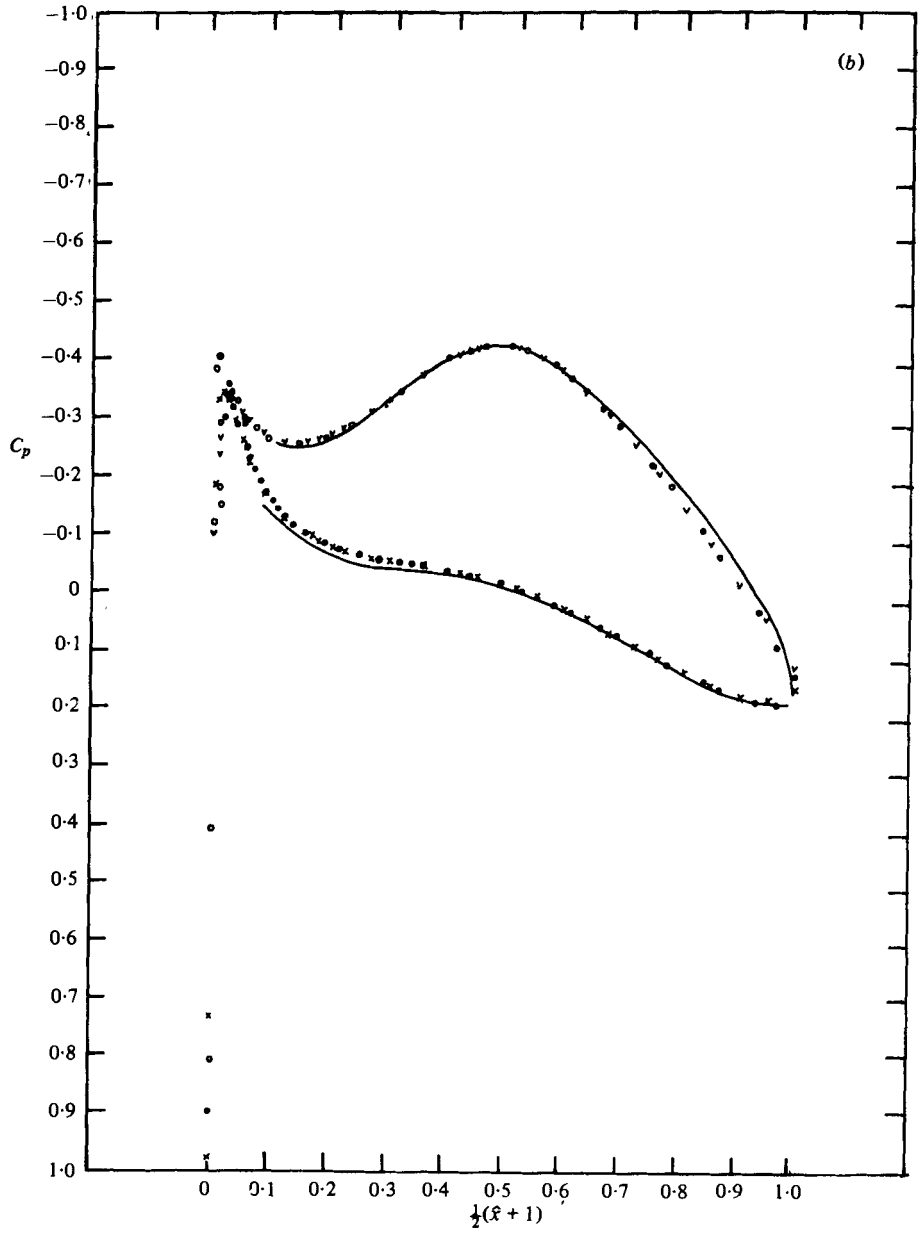

FIGURE 4(*b*). For legend see p. 551.

open circles; the corresponding FLO 22 data (from N.A.S.A. Ames) are presented as thin curves. The degree of agreement with the FLO 22 data are quite similar to that in the preceding comparisons. In this case, a small supercritical region appear in the aft wing panel, as anticipated (there are at least five surface grid points in the supercritical region). More extensive comparisons are given in Cheng & Meng (1979*b*).†

One major contribution to the 3D effect is the incidence correction which accounts

† Close examination of the FLO 22 data in this case reveals a slight spanwise fluctuation in surface pressure, attributable to an iterative convergence problem. The slightly larger discrepancies found in the c_p minimum and near the trailing edge may be related to the latter difficulty.

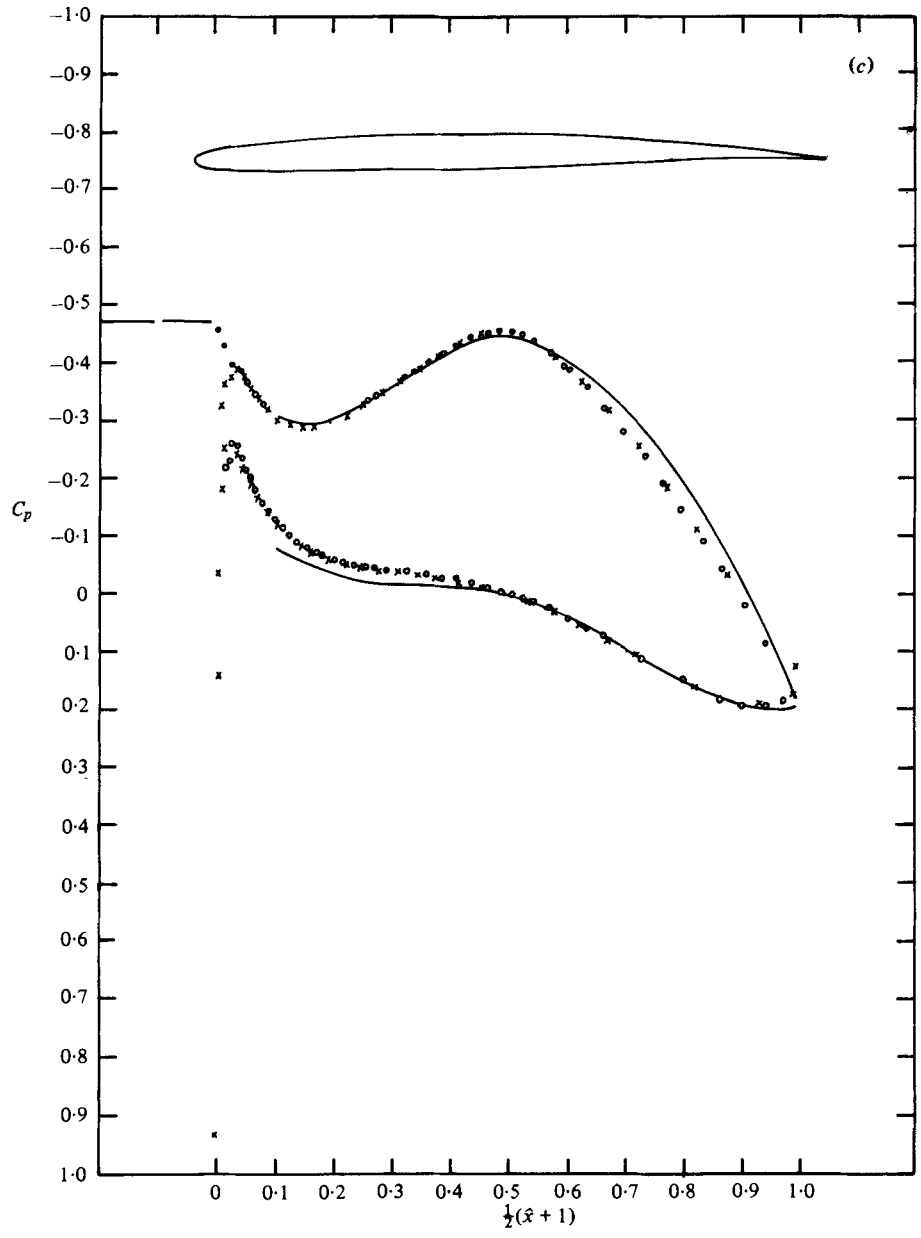

FIGURE 4. Comparison with a major-to-minor axes ratio of 20 at 22·5° sweep and a free-stream Mach number 0·8242. The present result is shown in solid curve. The C_p distribution at: (*a*) span station $\tilde{y} = -0{\cdot}69$; (*b*) span station $\tilde{y} = 0$; (*c*) span station $\tilde{y} = 0{\cdot}69$. ∨, ×, N.A.S.A. Ames (FLO 22); ○, ●, Grumman (FLO 22); ——, lifting line. $\alpha = 0°$, $\Omega = 22{\cdot}5°$, $AR_0 = 20$.

for the upwash induced by the far-wake vorticities, computed from $\bar{V}_I^{\infty}$ of (3.7*a*) via (3.7*b*) and (4.16*a*). The adequacy of this upwash calculation has already been demonstrated in examples pertaining to the linearized problem (Cheng 1978*a*, *b*); therefore, the good agreement reported here should not be too surprising.† Worthy of note in

† The scales of the span loading in figure 3 of Cheng 1978*a*, and in figures 4–6 of Cheng 1978*b*, should all be reduced by a factor of ten.

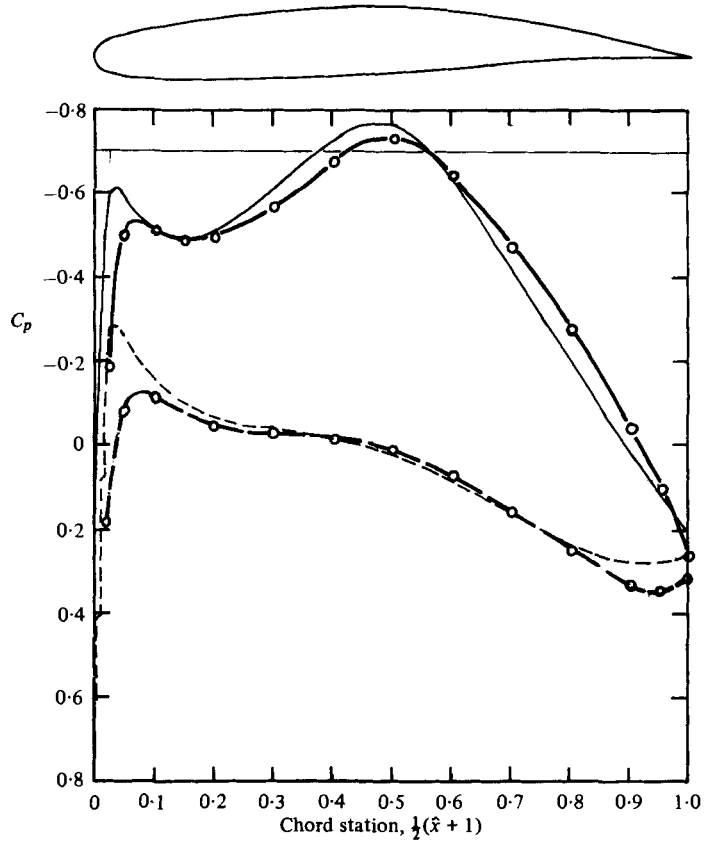

FIGURE 5. Comparison for a 12% thick, elliptic oblique wing with an axes ratio 14 at 30° yaw and $M_\infty = 0{\cdot}7677$. This graph gives surface C_p at span station $\tilde{y} = 0{\cdot}79$. N.A.S.A. Ames FLO 22: ——, upper; – – –, lower. Present theory: —○—, upper; – –○– –, lower.

this connexion is the use of the transonic similarity parameter $K_n = (1-M_n^2)/M_n\alpha^{\frac{2}{3}}$, and the retention of the $\cos\Lambda$ factor in computing $\tilde{\phi}_{0\tilde{x}}$ and c_p, which prove to be crucial in maintaining an accurate leading approximations, and are partly responsible for the good agreement achieved here.

It may be pointed out that existing 3D computer codes based on the full-potential equations do not satisfy exactly the condition across a trailing vortex sheet (Jameson 1974; Jameson & Caughey 1977). Thus, its validity also requires the small-disturbance assumption, strictly speaking. The value of the program lies, of course, on its ability to describe the flow field around the leading edge and near the trailing edge, where the small-disturbance approximation breaks down or becomes less accurate, assuming that problems of convergence with respect to mesh size, and to iteration, may not cause inaccuracy. The limitation on the computer storage available to the current 3D flow-field computation programs is well known. With this limitation, it is not clear whether the grid distributions in these programs are sufficiently refined for the purpose of describing the induced up-wash of the trailing vorticities in the far wake, so crucial to a high aspect-ratio wing. This uncertainty has been erased, in part, by the consistent comparisons shown above.

The study is supported by the U.S. Office of Naval Research, Fluid Dynamics Program. The numerical (FLO 22) data shown in the comparison study were made available to us through Mr Ronald C. Smith at N.A.S.A. Ames Research Center and Dr Rueben Chow at Grumman Aerospace Corporation. The senior author would like to thank Dr R. T. Jones for his helpful advice.

REFERENCES

ASHLEY, H. & LANDAHL, M. 1965 *Aerodynamics of Wings & Bodies*, pp. 137–142 and 227–244.

BALLHAUS, W. F. & GOORJIAN, P. M. 1977 *A.I.A.A. J.* **15**, 1728–1735.

BAUER, F., GARABEDIAN, P., KORN, D. & JAMESON, A. 1974 *Supercritical Wing Section*. II. Lectures notes in economics and mathematical systems, no. 108. Springer.

BOERSTOEL, J. W. 1974 *Nat. Aerosp. Lab. Rep.* NLRMP 74024 U. Amsterdam.

BUSEMANN, A. 1935 *Luftfahrtforschung* **12**, part 6.

CHENG, H. K. 1976 *Univ. So. Calif., School Engng, Dept. Aerosp. Engng Rep.* USCAE **133**.

CHENG, H. K. 1978*a* *A.I.A.A. J.* **16**, 1211–1213.

CHENG, H. K. 1978*b* *Univ. So. Calif., School Engng, Dept. Aerosp. Engng Rep.* USCAE 135.

CHENG, H. K. & HAFEZ, M. M. 1975 *J. Fluid Mech.* **72**, 161–187.

CHENG, H. K. & MENG, S. Y. 1979*a* *A.I.A.A. J.* **17**, 121–124.

CHENG, H. K. & MENG, S. Y. 1979*b* *Univ. So. Calif., School Engng, Dept. Aerosp. Engng Rep.* USCAE 136.

COLE, J. D. 1975 *SIAM J. Appl. Math.* **29**, 763–787.

COOK, P. 1978 *Indiana Univ. Math. J.* **27**, no. 1.

COOK, P. 1979 *Quart. Appl. Math.*, July, 178–202.

COOK, P. & COLE, J. D. 1978 *SIAM J. appl. Math.* **35**, 209–224.

COURANT, R. & HILBERT, D. 1965 *Methods of Mathematical Physics. II.* pp. 551–556.

EHLERS, F. E. 1974 *N.A.S.A. Rep.* CR-2257.

FUNG, K. Y., YU, N. J. & SEEBASS, R. 1978 *A.I.A.A. J.* **16**, 815–822.

HAFEZ, M. M. & CHENG, H. K. 1977*a* *A.I.A.A. J.* **15**, 329–331.

HAFEZ, M. M. & CHENG, H. K. 1977*b* *A.I.A.A. J.* **15**, 786–793.

HAFEZ, M. M., RIZK, X. & MURMAN, E. M. 1977 *Proc. AGARD Unsteady Transonic & Separated Flows*, Lisbon, Portugal.

JAMESON, A. 1974 *Comm. Pure Appl. Math.* **27**, 283–309.

JAMESON, A. & CAUGHEY, D. A. 1977 *New York Univ. ERDA Rep.* C00 3077–140.

JONES, R. T. 1946 *N.A.C.A. Rep.* no. 851.

JONES, R. T. 1971 *A.I.A.A. J.* **10**, 171–176.

JONES, R. T. 1977 *Acta Aeronautica* **4**, 99–110.

JONES, R. T. & COHEN, D. 1957 Aerodynamics of Wings at High Speed. In *Aerodynamic Components of Aircraft at High Speed* (ed. D. F. Donovan & H. R. Lawrence), pp. 3–236. Princeton University Press.

KACPRZYNSKI, J. J., OHMAN, L. H., GARABEDIAN, P. R. & KORN, D. G. 1971 *Nat. Res. Counc. Canada, Aero. Rep.* LR-554.

KÜCHEMANN, N. D. 1969 *Aeronautical J.* **73**, 101–110.

LANDAHL, M. 1962 *Symposium Transsonicum*, pp. 414–439.

MURMAN, E. M. 1974 *A.I.A.A. J.* **12**, 626–633.

MURMAN, E. M. & COLE, J. D. 1971 *A.I.A.A. J.* **9**, 114–121.

MURMAN, E. M. & KRUPP, J. A. 1971 *Proc. 2nd Int. Conf. Numerical Methods in Fluid Dynamics*, Lecture notes in physics, vol. 8, pp. 199–206. Springer.

NIEUWLAND, G. Y. 1967 *NLR (Neth.) Tech. Rep.* T 172.

OSWATITSCH, K. 1962 *Symposium Transsonicum*, pp. 402–413.

OSWATITSCH, K. & ZIEREP, J. 1960 *Z. angew. Math. Mech. Suppl.* **40**, 143–144.

PRANDTL, L. 1918 Nachrichten d.k. Gesellschaft d. Wiss. zu Göttingen, *Math-Phys. Klasse*, pp. 451–477.

SPRIETER, J. R. 1953 *N.A.C.A. Rep.* 1153.

TIMMAN, R. 1962 *Symposium Transsonicum*, pp. 394–401.

TRACI, R. M., ALBANO, E. D. & FARR, J. L. 1976 *A.I.A.A. J.* **4**, 1258–1265.

VAN DYKE, M. D. 1964 *Perturbation Methods in Fluid Mechanics*, pp. 167–176. Academic.

WHITCOMB, R. T. 1974 Paper presented at the *9th Int. Congr. Aero. Sci.*, Haifa, Israel.

WILLIAMS, M. H. 1979 *A.I.A.A. J.* **17**, 394–397.